

Electrokinetic oscillatory flow and energy conversion of viscoelastic fluids in microchannels: a linear analysis

Zhaodong Ding¹ and Yongjun Jian^{1,†}

¹School of Mathematical Science, Inner Mongolia University, Hohhot, Inner Mongolia 010021, PR China

(Received 4 June 2020; revised 16 March 2021; accepted 26 April 2021)

We studied the electrokinetic flow of viscoelastic fluids subjected to an oscillatory pressure gradient. Under the assumption of laminar unidirectional flow, the constitutive and motion equations of fluids are in the linear regime. Since the surface potentials are assumed to be small, the Poisson–Boltzmann equation is linearised. Resonance behaviours appear in the flow when the elastic effect of fluids is dominant. Based on the interaction of viscoelastic shear waves, we explain the mechanism of resonance and derive the critical Deborah number, $De_c = 1/4$, which dictates the occurrence of resonance. Using the Maxwell fluid model, the resonance enhances the electrokinetic effects and dramatically increases the electrokinetic energy conversion efficiency. However, by employing the Oldroyd-B fluid model, we reveal that the amplification of efficiency is suppressed even for a very small Newtonian solvent contribution. This could be one of the reasons for the unavailability of reports on experimental verification regarding the high efficiency predicted by Bandopadhyay & Chakraborty (*Appl. Phys. Lett.*, vol. 101, 2012, 043905). The damping effect of solvent viscosity is more significant for higher-order resonances. The effects of multiple relaxation times on the resonance behaviours are investigated and the results indicate that De_c still dominates the occurrence of resonances for streaming potential field and flow rate.

Key words: microfluidics, viscoelasticity

1. Introduction

The transport processes where a charged mobile layer interacts with or induces electric fields due to the relative motion between substrate and solution are collectively termed electrokinetics (Hunter 2000). In recent decades, electrokinetic phenomena, including electro-osmosis, streaming potential, electrophoresis and sedimentation potential, have

[†] Email address for correspondence: jianyj@imu.edu.cn

attracted significant attention and provided many applications in micro- and nanochannels (Schoch, Han & Renaud 2008; Sparreboom, van den Berg & Eijkel 2010; Guan, Li & Reed 2014). The presence of a charged layer close to a solid–liquid interface is pivotal to all electrokinetic phenomena. Most solids spontaneously acquire surface electric charges when brought into contact with a polar medium (Li 2004; Masliyah & Bhattacharjee 2006). These charges are screened by the accumulation of counter-ions near the surface, to form a Stern layer and a diffuse layer, which constitute the so-called electrical double layer (EDL). The characteristic thickness of the EDL is commonly known as the Debye length (Jian *et al.* 2017). The charged walls of a channel are increasingly important in micro-/nanoscales because of the higher surface-to-volume ratio (Bocquet & Charlaix 2010). When a liquid is forced to flow through a channel by applying a pressure difference, there is a net flux of ions downstream in the EDL adjacent to the channel walls. This is called streaming current or advection current. The accumulation of charges at the channel downstream creates an electrical potential difference between the two ends of the channel. This potential difference is termed the streaming potential, and it depends on the surface charge, electrolyte concentration and channel dimension (Das, Guha & Mitra 2013). This streaming potential field, in turn, generates a current known as the conduction current, which flows against the direction of the pressure-driven flow. The total current within the cell is only zero if there is no external path for the current, which is often referred to as electroneutrality of current (Goswami & Chakraborty 2010).

Streaming potential phenomena are relevant in suspension rheology (Russel 1978; Sherwood 1980), geophysical two-phase flows through fine porous media (Bolève *et al.* 2007; Sherwood 2007, 2008, 2009; Lac & Sherwood 2009) and accurate measurement of zeta potentials (Lyklema 1995). They provide a mechanism for converting mechanical energy into electrical energy. Such a mechanism is called electrokinetic energy conversion (EKEC). The idea of harvesting electrical energy from a fluidic system is not new (Osterle 1964). However, it has attracted significant attention recently owing to rapid advancements in micro- and nanofluidics (Daiguji *et al.* 2004; van der Heyden *et al.* 2006, 2007; Xuan & Li 2006; Wang & Kang 2010; Chang & Yang 2011; Gillespie 2012; Siria *et al.* 2013). Especially, nanoscale fluidic devices allow probing of the regime of EDL overlaps where the EKEC efficiency is expected to be the highest (Pennathur, Eijkel & van den Berg 2007). Although the energy harnessed from a single nanochannel may be rather small, this effect can be substantially magnified by employing arrays of nanopores or macroscopic nanoporous materials (Yang *et al.* 2003; Daiguji *et al.* 2006).

Currently, experimental EKEC efficiency is relatively low. For example, the highest efficiency of about 3% was reported by van der Heyden *et al.* (2007) for a channel of 75 nm in height with a dilute KCl aqueous solution in a steady pressure-driven flow. To improve the EKEC efficiency, several studies have employed wall slip (Davidson & Xuan 2008a; Ren & Stein 2008), soft nanochannels (Chanda, Sinha & Das 2014; Patwary, Chen & Das 2016), steric effect (Bandopadhyay & Chakraborty 2011), time-periodic pressure (Goswami & Chakraborty 2010), polymer addition (Nguyen *et al.* 2013), buffer anion effect (Mei, Yeh & Qian 2017), transverse magnetic fields (Munshi & Chakraborty 2009) and layering of large ions near the wall–liquid interface (Gillespie 2012). Bandopadhyay & Chakraborty (2012) reported a mechanism for very large augmentation in the energy-harvesting capabilities of nanofluidic devices through the combined deployment of viscoelastic fluids and oscillatory driving pressure forces. They found that when the forcing frequency of a pressure-driven flow matches with the inverse of the relaxation time scale of a typical viscoelastic fluid, the EKEC efficiency could be highly amplified due to the complex interplay between fluid rheology and ionic transport

within the EDL, which can be attributed to the viscoelastic resonance phenomenon. Specifically, they predicted that for a slit-type microchannel ($\kappa h = 500$, with half-channel height h and Debye length $1/\kappa$), the conversion efficiency can be of the order of 10%, and that for a nanochannel ($\kappa h = 10$), without considering the surface conductance, the conversion efficiency could even be higher than 95%. This result is controversial, and the mechanism of enhancement needs to be further explored. On the one hand, as remarked by Nguyen *et al.* (2017), the efficiency defined by Bandopadhyay & Chakraborty is the thermodynamic efficiency, where no actual power is delivered by the system. The maximal efficiency at maximal output power in a load resistor is more relevant, and it is to the tune of 24% for a nanochannel (Nguyen *et al.* 2017). Within the linear response regime of electrokinetic flows, it is proved that this maximum efficiency cannot exceed 50% based on thermodynamic analyses (Xuan & Li 2006; Ding, Jian & Tan 2019). On the other hand, the model used by Bandopadhyay & Chakraborty is a simple Maxwell one that is a considerable simplification of viscoelastic fluids and only valid at low shear rates and frequencies (Castrejón-Pita *et al.* 2003). Some significant deviations in the Maxwell behaviour are observed for intermediate- and high-frequency regimes for wormlike micellar solutions due to the Rouse-like behaviour of the individual entangled segments (Yesilata, Clasen & Mckinley 2006) and additional solvent stress (Casanellas & Ortín 2012).

To clarify the fundamental aspects of resonance phenomena in electrokinetic oscillatory flows of viscoelastic fluids, we employ a generic constitutive model and provide a detailed analysis in the linear regime. In practice, a viscoelastic fluid is usually a suspension formed by various polymers or a solution with fine additives. The macroscopic description of viscoelastic fluids combines elastic behaviour, represented by an elastic spring, and viscous behaviour, represented by a dissipative dashpot. Depending on the precise configuration of these primary elements, one can obtain different constitutive equations (e.g. the Maxwell, Oldroyd-B, Giesekus, Phan-Thien–Tanner and Johnson–Segalman models). For polymer aqueous solutions, the effect of solvent composition can be investigated using the Oldroyd-B model, which represents a solution of a Maxwellian viscoelastic fluid with a single relaxation time λ solved in a Newtonian solvent with constant viscosity (Bird, Armstrong & Hassager 1987).

The laminar oscillatory flows of Maxwell and Oldroyd-B viscoelastic fluids have been investigated by Casanellas & Ortín (2011), and they exhibit many interesting features absent in the flows of Newtonian fluids. Barnes, Townsend & Walters (1969) investigated the effect of an oscillatory pressure gradient around a non-zero mean in straight cylinders. The experimental results obtained for dilute aqueous solutions of polyacrylamide show a dramatic increase in the mean flow rate at particular values of the mean pressure gradient, because of the ‘resonance’ effect between fluid elasticity and oscillatory driving. Their observations qualitatively agree with their theoretical predictions based on the power series expansion of the velocity and shear rate of a fluid characterised by apparent viscosity. Several authors used different fluid models to study the mechanisms for flow enhancement (Barnes, Townsend & Walters 1971; Davies, Bhumiratana & Bird 1978; Phan-Thien 1978, 1980, 1981; Manero & Walters 1980; Phan-Thien & Dudek 1982a,b; Siginer 1991; Andrienko, Siginer & Yanovsky 2000; Herrera 2010).

The steady and transient flows of most polymeric solutions and melts cannot be adequately described by single-mode differential constitutive equations (Bird *et al.* 1987). Thus, there is a need to employ multimode constitutive equations to obtain a better description of real fluids, which possess a spectrum of relaxation times instead of a single characteristic time scale. The concept has existed for more than a century in the form

of the generalised Maxwell model for linear viscoelasticity (Sadek & Pinho 2019). In particular, the Rouse-like behaviour of dilute polymer solutions, as previously mentioned, can be expressed by the generalised Maxwell model. Prost-Domasky & Khomami (1996) analysed the start-up of plane Couette flow and large-amplitude oscillatory shear flow of single-mode and multimode Maxwell fluids as well as Oldroyd-B fluids using analytical or semi-analytical methods. Andrienko *et al.* (2000) investigated the resonance behaviour of a fluid described by the upper-convected Maxwell (UCM) model with a discrete spectrum of relaxation times. Moyers-Gonzalez, Owens & Fang (2008, 2009) proposed a non-homogeneous haemorheological model for human blood, where the effect of multiple relaxation times was introduced. Sadek & Pinho (2019) presented an analytical solution for the electro-osmotic oscillatory flow of multimode UCM fluids in small-amplitude oscillatory shear.

In this work, we introduce a multimode model to investigate the streaming potential and EKEC of viscoelastic fluids. The strain–stress relationship is expressed as follows:

$$\left. \begin{aligned} T &= T_s + T_p, \\ T_s &= \eta_s \dot{\gamma}, \quad T_p = \sum_{k=1}^N T_k, \\ T_k + \lambda_k \overset{\nabla}{T}_k &= \eta_k \dot{\gamma}. \end{aligned} \right\} \quad (1.1)$$

Here, T denotes the Cauchy stress tensor, which is decomposed into a polymer contribution T_p and a Newtonian solvent contribution T_s , and $\dot{\gamma} = \nabla V + (\nabla V)^\dagger$ is the rate-of-strain tensor with the fluid velocity V . The superscript ∇ denotes the upper-convected derivative and

$$\overset{\nabla}{T} = \frac{\partial T}{\partial t} + V \cdot \nabla T - (\nabla V)^\dagger \cdot T - T \cdot \nabla V. \quad (1.2)$$

In (1.1), the symbols N , λ_k and η_k ($k = 1, \dots, N$) denote the number of relaxation times in the spectrum, the k th relaxation time and the k th partial viscosity, respectively, and η_s is the constant viscosity of the Newtonian solvent. The contribution of polymer viscosity can be expressed in terms of the partial viscosity as $\eta_p = \sum \eta_k$, and the total viscosity of the solution is given by the sum of the solvent and polymer contributions, $\eta = \eta_s + \eta_p$. The solvent viscosity fraction, η_s/η , is denoted by X , which is also known as the dimensionless retardation time (Casanellas & Ortín 2011).

This model is a multimode formulation of the UCM model. An important feature of this model is that it allows for a spectrum of relaxation times and contains the Newtonian solvent stress. For $N = 1$ (i.e. single relaxation time), the Oldroyd-B model is obtained. Furthermore, for $N = 1$ and $X = 0$, the Newtonian solvent contribution vanishes and this model is simplified to the UCM model. The other limiting behaviour is attained at $X = 1$, where the elastic contribution of the polymer vanishes and the Newtonian relation is recovered. For unidirectional flows, the presented model has a linear strain–stress equation, and it fails in predicting nonlinear features (e.g. shear-thinning behaviour) that appear at considerably large shear rates in viscoelastic fluids. It is a good approximation of viscoelastic fluids at small shear rates and can capture the resonance behaviour of viscoelastic fluids, which is of interest to us.

Two relevant dimensionless numbers in viscoelastic flows are the Deborah (De) and Weissenberg (Wi) numbers (Morozov & van Saarloos 2007). The Deborah number sets the interplay between the characteristic relaxation time of fluids and the viscous diffusion

time, and it is defined as

$$De = \lambda_{max}\eta/\rho h^2 = \lambda_{max}/t_v, \tag{1.3}$$

where λ_{max} is the largest relaxation time, ρ the fluid density, h the channel dimension and $t_v = \rho h^2/\eta$ the characteristic time of purely viscous effects. The above definition of De generalises that employed by del Río, de Haro & Whitaker (1998) for multiple relaxation times. As $De \rightarrow 0$, the fluid relaxes much faster than the typical time scale of the flow and the Newtonian flow behaviour is recovered. For $De > 1$, the relaxation time of the fluid is larger than the time scale of the flow and the fluid elasticity dominates the flow behaviour. In shear flows, viscoelastic fluids are also subject to shear-driven normal stresses. The ratio of the normal and shear stresses quantifies the nonlinear response of the viscoelastic fluid, and it is proportional to Wi (Galindo-Rosales *et al.* 2014), which is defined based on the largest relaxation time and the maximum local shear rate in this paper as

$$Wi = \lambda_{max}\dot{\gamma}_{max}. \tag{1.4}$$

Analogous to the Reynolds (Re) number in Newtonian fluids, as Wi increases, different flow regimes can be explored in viscoelastic fluids (Morozov & van Saarloos 2007). For $Wi < 1$, the fluid exhibits laminar shear flows and the fluid response to external forces is expected to be linear, whereas, for $Wi > 1$, nonlinearities start to manifest. In the high- Wi regime, elastic instability and secondary flows are likely to appear (Torralba *et al.* 2007).

In this study, we focused on the electrokinetic phenomena induced by an oscillatory flow based on the viscoelastic model, including the effects of a Newtonian solvent and multiple relaxation times. Some restrictions, such as low Wi and surface potential, have been proposed to keep the fluid response to the pressure gradient and streaming potential in the linear regime, which makes it relatively easy to solve the governing equations, and thereby allows a detailed mathematical analysis of the resonance behaviour. The remainder of this paper is organised as follows. In § 2 the problem of the study is formulated and analytical solutions of the fluid velocity and EDL potential are presented. The streaming potential and EKEC efficiency are expressed and further analysed. The elastic resonance behaviours of related physical quantities are presented and characterised in § 3. The effects of solvent viscosity and multiple relaxation times on the resonance behaviours are investigated in §§ 3.1 and 3.2, respectively. The validity of the linear analysis is examined in § 4. Finally, the study is summarised and concluded in § 5.

2. Theoretical formulation

We consider the electrokinetic transport between two infinitely large parallel plates with a separation of $2h$. The fluid medium is viscoelastic, modelled by (1.1), and it is driven by a harmonically oscillating pressure gradient (figure 1). A Cartesian system (x, y, z) is constructed, such that the x - z plane is parallel to the surface of the plate with the origin at the middle of the microchannel, the x axis is consistent with the direction of the pressure gradient (axial direction) and the y axis is perpendicular to the plates (transverse direction). The flow is expressed by the Navier–Stokes equation with an additional electrical body force and the continuity equation for an incompressible fluid:

$$\left. \begin{aligned} \rho \frac{\partial V}{\partial t} + \rho(V \cdot \nabla)V &= -\nabla p + \nabla \cdot T + F_{EK}, \\ \nabla \cdot V &= 0. \end{aligned} \right\} \tag{2.1}$$

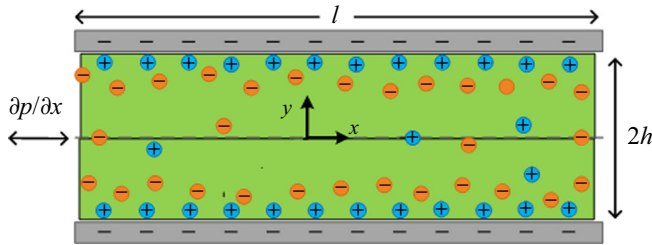


Figure 1. Schematic diagram of a microchannel filled with a fluid medium. The EDL forms at the interior of negatively charged walls. Periodic pressure gradient is applied along the channel in the x direction.

In the above equation, $V = (u, v, w)$ denotes the fluid velocity vector and F_{EK} is the electrokinetic body force, which is given by (Karniadakis, Beskok & Aluru 2005)

$$F_{EK} = \rho_e E - \frac{1}{2} E \cdot E \nabla \epsilon + \frac{1}{2} \nabla \left(\rho \frac{\partial \epsilon}{\partial \rho} E \cdot E \right), \quad (2.2)$$

where ϵ is the permittivity of the medium, E is the electric field which is related to the electric potential ϕ by $E = -\nabla \phi$, $\rho_e = e \sum_i z_i n_i$ is the local net charge density, e is the electronic charge and n_i and z_i are the number density and valence of ion i , respectively. Considering the constant permittivity of the medium, (2.2) reduces to $F_{EK} = \rho_e E$.

When a fluid contains charged ionic species, the movement or mass transfer of the anions and cations in the fluid flow is of interest. Generally, the ionic flux satisfies the advection–diffusion–migration equation (i.e. the Nernst–Planck equation), given by

$$j_i = n_i V - D_i \nabla n_i - \frac{z_i e n_i D_i}{k_B T} \nabla \phi. \quad (2.3)$$

Here, D_i is the diffusivity of ions in the solution, k_B the Boltzmann constant, T the absolute temperature and ϕ the total electric potential. The first term on the right-hand side of (2.3) is the flux due to bulk convection, the second term is that due to concentration gradient (i.e. diffusion process) and the last term is that due to migration.

2.1. Electric potential distribution

The electric potential at a location (x, y) in the channel, given by $\phi(x, y, t)$, arises due to the superposition of the induced external electric potential (streaming potential) and the potential due to surface charges on the microchannel walls (EDL potential). Assuming that the EDL potential is independent of the axial position in the microchannel (which is valid for long microchannels, neglecting any end effects), the total electric potential can be expressed as follows:

$$\phi(x, y, t) = \psi(y) + [\phi_0 - xE_s(t)], \quad (2.4)$$

where $\psi(y)$ is the EDL potential due to the EDL at the equilibrium state corresponding to no fluid motion and no external electric field, $\phi_s \equiv \phi_0 - xE_s(t)$ is the streaming electric potential at a given axial location due to the electric field strength E_s in the absence of the EDLs, ϕ_0 is the reference value of the potential at $x = 0$ and E_s is the streaming potential field that is independent of the position but dependent on time since E_s is closely related to the fluid velocity, which is time-dependent (see §§ 2.2 and 2.3). Note that (2.4) is analogous to (8.2) of Masliyah & Bhattacharjee (2006), where E_s is independent of time.

The local net charge density ρ_e is related to the electric potential ϕ through the Poisson equation as follows:

$$\nabla^2 \phi = -\frac{\rho_e}{\varepsilon}. \quad (2.5)$$

Introducing (2.4) into the Poisson equation, we obtain the following equation for the slit microchannel:

$$\frac{d^2 \psi}{dy^2} = -\frac{\rho_e}{\varepsilon}. \quad (2.6)$$

Considering the zero flux of ions in the y direction at equilibrium, (2.3) gives

$$j_{i,y} = n_i v - D_i \frac{dn_i}{dy} - \frac{z_i e n_i D_i}{k_B T} \frac{d\psi}{dy} = 0. \quad (2.7)$$

Furthermore, as $v = 0$ for laminar parallel flows, one can derive the Boltzmann distribution for the ionic number concentration near a charged surface from (2.7), i.e.

$$n_i = n_{i\infty} \exp\left(-\frac{z_i e \psi}{k_B T}\right), \quad (2.8)$$

where $n_{i\infty}$ denotes the bulk number density of ion i at the neutral state where $\psi = 0$. Combining (2.6) and (2.8), we obtain the Poisson–Boltzmann equation for the slit microchannel as follows:

$$\frac{d^2 \psi}{dy^2} = -\frac{e}{\varepsilon} \sum_i z_i n_{i\infty} \exp\left(-\frac{z_i e \psi}{k_B T}\right). \quad (2.9)$$

Since it is difficult to analytically solve the full set of electrokinetic equations, three main approximation methodologies have been developed over the years, which are appropriate for low surface electric potential, weak field or flow and thin double layers, respectively. For example, the thin-double-layer limit was employed by Yariv, Schnitzer & Frankel (2011), Schnitzer, Frankel & Yariv (2012) and Schnitzer & Yariv (2016) to investigate streaming potential phenomena. However, this approximation cannot be applied to nanochannels where the EDL thickness is comparable to the size of the channel. In this study, we employed the low-surface-potential assumption, i.e. $|z_i e \psi / k_B T| < 1$, so that the Debye–Hückel approximation can be applied to (2.9) to obtain the following equation (see Masliyah & Bhattacharjee 2006):

$$\frac{d^2 \psi}{dy^2} = \kappa^2 \psi, \quad (2.10a)$$

where

$$\kappa^2 = \frac{e^2}{\varepsilon k_B T} \sum_i n_{i\infty} z_i^2. \quad (2.10b)$$

The Debye length is $1/\kappa$, which characterises the EDL thickness (typically ≈ 10 nm). Equation (2.10a) is the linearised version of the Poisson–Boltzmann equation and gives a satisfactory EDL potential profile (even when linearisation is unjustifiable).

With the above basic geometry, the EDL potential varies only along the y axis, and the appropriate boundary conditions are

$$\psi = \zeta, \quad \text{at } y = \pm h, \tag{2.10c}$$

where ζ is the zeta potential at the walls. Thus, the solution to (2.10a) subject to the conditions in (2.10c) is given as follows:

$$\psi(y) = \zeta \frac{\cosh(\kappa y)}{\cosh(\kappa h)}, \quad -h \leq y \leq h. \tag{2.11}$$

To determine the streaming potential field in (2.4), the velocity field and the condition of electroneutral current are required. The expression of the streaming potential field and its analysis are presented in § 2.3.

2.2. Fluid velocity and flow rate

For the velocity field, the laminar regime is achieved by applying a small driving ($Wi < 1$), which corresponds to small amplitudes of the imposed pressure gradient (Casanellas & Ortín 2011, 2012). Thus the flow is parallel to the walls and along the x direction. The velocity is assumed to be $V = (u(y, t), 0, 0)$ and the continuity equation is satisfied automatically. The strain–stress relationship (1.1) of viscoelastic fluids is linear for this unidirectional flow, and on substituting it into the Navier–Stokes equation, we obtain

$$\left. \begin{aligned} \rho \frac{\partial u}{\partial t} &= -\frac{\partial p}{\partial x} + \eta_s \frac{\partial^2 u}{\partial y^2} + \sum_{k=1}^N \frac{\partial \tau_k}{\partial y} + \rho_e E_s, \\ \left(1 + \lambda_k \frac{\partial}{\partial t}\right) \tau_k &= \eta_k \frac{\partial u}{\partial y}, \end{aligned} \right\} \tag{2.12a}$$

where τ_k is the xy component of T_k and $E_s = -\partial\phi_s/\partial x$ is the streaming potential field along the x direction, which is considered to be uniform in the channel. Assuming a harmonic pressure gradient, $\partial p/\partial x = \cos(\omega t) dp_0/dx = \text{Re}(dp_0/dx \exp(i\omega t))$ using complex variables, where dp_0/dx is the amplitude of the applied pressure gradient and ω the frequency of oscillation. The velocity field, stress tensor and streaming potential field can be written in complex forms as follows:

$$u(y, t) = \text{Re}(u_0(y) e^{i\omega t}), \quad \tau_k(y, t) = \text{Re}(\tau_k^0(y) e^{i\omega t}), \quad E_s(t) = \text{Re}(E_0 e^{i\omega t}), \tag{2.12b}$$

where Re denotes the real part of a complex number. Substituting these expressions into (2.12a), we obtain

$$\left. \begin{aligned} i\rho\omega u_0 &= -\frac{dp_0}{dx} + \eta_s \frac{d^2 u_0}{dy^2} + \sum_{k=1}^N \frac{d\tau_k^0}{dy} + \rho_e E_0, \\ (1 + i\omega\lambda_k)\tau_k^0 &= \eta_k \frac{du_0}{dy}. \end{aligned} \right\} \tag{2.13}$$

Introducing the following dimensionless groups:

$$\left. \begin{aligned} Y = \frac{y}{h}, \quad \Psi = \frac{\psi}{\zeta}, \quad X = \frac{\eta_s}{\eta}, \quad \xi_k = \frac{\eta_k}{\eta}, \quad \bar{\omega} = \omega\lambda_{max}, \quad K = \kappa h, \\ \bar{E}_0 = \frac{E_0}{E_m}, \quad \bar{u}_0 = \frac{u_0}{u_m}, \quad \text{with } u_m = -\frac{h^2}{\eta} \frac{dp_0}{dx} \text{ and } E_m = -\frac{h^2}{\varepsilon\xi} \frac{dp_0}{dx}, \end{aligned} \right\} \tag{2.14}$$

and eliminating τ_k^0 from (2.13), we obtain

$$\begin{aligned} \frac{d^2 \bar{u}_0}{dY^2} - \frac{i\bar{\omega}}{De} \left(X + \sum_{k=1}^N \frac{\xi_k}{1 + i\omega\lambda_k} \right)^{-1} \bar{u}_0 \\ = \left(X + \sum_{k=1}^N \frac{\xi_k}{1 + i\omega\lambda_k} \right)^{-1} \left[-1 + K^2 \bar{E}_0 \frac{\cosh(KY)}{\cosh(K)} \right]. \end{aligned} \quad (2.15)$$

Here, $\rho_e = -\varepsilon\kappa^2\psi$ is used, $\bar{\omega}$ is the non-dimensional frequency, K the inverse of the normalised EDL thickness and De the Deborah number defined in (1.3). Furthermore, by defining the dimensionless parameter

$$\alpha = \sqrt{-\frac{i\bar{\omega}}{De} \left(X + \sum_{k=1}^N \frac{\xi_k}{1 + i\omega\lambda_k} \right)^{-1/2}}, \quad (2.16)$$

the solution to (2.15) subject to the no-slip conditions at walls can be expressed as follows:

$$\begin{aligned} \bar{u}_0(Y) = \frac{De}{i\bar{\omega}} \left[1 - \frac{\cos(\alpha Y)}{\cos(\alpha)} \right] - \frac{\alpha^2 De K^2 \bar{E}_0}{i\bar{\omega}(K^2 + \alpha^2)} \left[\frac{\cosh(KY)}{\cosh(K)} - \frac{\cos(\alpha Y)}{\cos(\alpha)} \right] \\ \triangleq \bar{u}_{P0}(Y) + \bar{u}_{E0}(Y) \cdot \bar{E}_0. \end{aligned} \quad (2.17)$$

Equation (2.17) gives the complex amplitude of the axial velocity. The first term is the liquid velocity due to the imposed pressure gradient and the second term represents the additional convective transport of the fluid medium due to the induced streaming potential field. Then, the complex amplitude of the dimensionless flow rate (per unit width of the channel) scaled by hu_m is given as follows:

$$\begin{aligned} \bar{Q}_0 = 2 \int_0^1 \bar{u}_0(Y) dY = \frac{2De}{i\bar{\omega}} \left[1 - \frac{\tan(\alpha)}{\alpha} \right] - \frac{2\alpha^2 De K^2 \bar{E}_0}{i\bar{\omega}(K^2 + \alpha^2)} \left[\frac{\tanh(K)}{K} - \frac{\tan(\alpha)}{\alpha} \right] \\ \triangleq \bar{Q}_{P0} + \bar{Q}_{E0}. \end{aligned} \quad (2.18)$$

2.3. Streaming potential field and scaling laws

As stated in the Introduction section, when a flow is driven by a pressure gradient, a streaming current and streaming potential can be established and pressure-to-voltage energy conversion can be achieved. Using (2.3), the current density in the x direction can be expressed as

$$i_x = e \sum_i z_i j_{i,x} + \frac{\sigma_{Stern}}{h} E_s = eu \sum_i z_i n_i - e \sum_i D_i z_i \frac{\partial n_i}{\partial x} + \frac{e^2}{k_B T} E_s \sum_i z_i^2 D_i n_i + \frac{\sigma_{Stern}}{h} E_s. \quad (2.19)$$

An additional term (the last term), which accounts for the Stern layer conductance with a surface conductivity σ_{Stern} , is introduced into the traditional equation of current density (Davidson & Xuan 2008b). The total current per unit width of the slit channel is given by

$$I = 2 \int_0^h i_x dy. \quad (2.20)$$

For simplicity, we consider a symmetric electrolyte ($z_+ = -z_- = z$) with the same ionic diffusion coefficients D . In the present flow system, it is assumed that the ionic

concentration does not vary along the length of the channel. Consequently, $\partial n_i / \partial x = 0$ and the second term of (2.19) is eliminated. Thus, the current density reduces to

$$\begin{aligned} i_x &= zeu(n_+ - n_-) + \frac{e^2 z^2 D}{k_B T} E_s (n_+ + n_-) + \frac{\sigma_{Stern}}{h} E_s \\ &= \rho_e u + \sigma_b \cosh\left(\frac{ze\psi}{k_B T}\right) E_s + \frac{\sigma_{Stern}}{h} E_s, \end{aligned} \quad (2.21a)$$

where the Boltzmann distribution in (2.8) is employed, and the local (σ) and bulk (σ_b) conductivities of the fluid are expressed as follows:

$$\sigma = \sigma_b \cosh\left(\frac{ze\psi}{k_B T}\right) \quad \text{and} \quad \sigma_b = \frac{2e^2 z^2 n_\infty D}{k_B T}. \quad (2.21b)$$

Note that the factor $\cosh(ze\psi/k_B T)$ reflects the influence of diffuse charge cloud on the bulk conductivity.

Applying the Taylor series for the cosh term in (2.21b),

$$\cosh\left(\frac{ze\psi}{k_B T}\right) = 1 + \frac{1}{2!} \left(\frac{ze\psi}{k_B T}\right)^2 + O(\psi^4), \quad (2.22)$$

we find that the local conductivity is a modification of $O(\zeta^2)$ in the case of bulk conductivity because of the presence of the diffuse layer. Therefore, the effect of diffuse charges on bulk conductivity can be ignored when assuming a low surface potential; then, $\sigma \approx \sigma_b$.

To evaluate the relative importance of Stern layer conductance and bulk conductance, we introduce the Dukhin number, $Du = \sigma_{Stern}/h\sigma_b$. From (2.21b), we have that $Du = \sigma_{Stern}/h\Lambda c_b$, where c_b is the ionic concentration of the bulk fluid and $\Lambda = 2e^2 z^2 N_A D/k_B T$ is the molar conductivity with N_A the Avogadro number. To examine quantitatively the effect of Stern layer conductance, we consider a KCl solution with $c_b = 10^{-4}$ M as an example. The ionic diffusion coefficient D is approximately equal to 1.9×10^{-9} m² s⁻¹ (Daiguji *et al.* 2004). The molar conductivity Λ is calculated to be 0.0144 S m² mol⁻¹ at temperature $T = 298$ K (Davidson & Xuan 2008b). The half-height of the channel $h = 1$ μm. The value of σ_{Stern} ranges from 10 to 30 pS, according to the experiment of van der Heyden *et al.* (2007). Thus, the Dukhin number is between 0.01 and 0.03. This indicates that the Stern layer conductance has an important effect only at very small channel size and extremely low ionic concentration ($< 10^{-4}$ M). Here, we ignore the influence of the Stern layer conductance.

Integrating the current density over the channel section in (2.20) and applying the complex forms in (2.12b), the complex amplitude of the total ionic current can be obtained:

$$I_0 = 2 \int_0^h \rho_e u_0 dy + 2h\sigma_b E_0. \quad (2.23a)$$

From this, the amplitudes of the streaming and conduction currents through the channel can be obtained, respectively, as

$$I_{s0} = 2 \int_0^h \rho_e u_0 dy \quad \text{and} \quad I_{c0} = 2h\sigma_b E_0. \quad (2.23b)$$

Using the condition of electroneutral current ($I_{s0} + I_{c0} = 0$), dimensionless variables (2.14) and velocity field (2.17), the amplitude of the dimensionless streaming potential

field can be expressed as

$$\bar{E}_0 = \frac{\int_0^1 \Psi(Y) \bar{u}_{P0}(Y) dY}{R - \int_0^1 \Psi(Y) \bar{u}_{E0}(Y) dY}, \quad (2.24)$$

where

$$R = \frac{\eta D}{\varepsilon \zeta^2} \quad (2.25)$$

is the inverse ionic Péclet number, characterising the ratio of the conduction current to the streaming current (Chakraborty & Das 2008; Chanda *et al.* 2014). Using the analytical solutions of the velocity and the EDL potential Ψ , we obtain

$$\int_0^1 \Psi(Y) \bar{u}_{P0}(Y) dY = \frac{\alpha De}{i\bar{\omega}(K^2 + \alpha^2)} \left[\frac{\alpha}{K} \tanh(K) - \tan(\alpha) \right] \quad (2.26a)$$

and

$$\begin{aligned} & \int_0^1 \Psi(Y) \bar{u}_{E0}(Y) dY \\ &= -\frac{\alpha^2 K^2 De}{i\bar{\omega}(K^2 + \alpha^2)} \left[\frac{2K + \sinh(2K)}{4K \cosh^2(K)} - \frac{K \sinh(K) \cos(\alpha) + \alpha \cosh(K) \sin(\alpha)}{(K^2 + \alpha^2) \cosh(K) \cos(\alpha)} \right]. \end{aligned} \quad (2.26b)$$

For viscous fluids (e.g. Newtonian fluids), the effect of the induced streaming potential on the velocity is negligible compared with that of the pressure gradient (i.e. $\bar{u}_0 \approx \bar{u}_{P0}$) (see figure 5 for low De). Thus, the streaming potential field in (2.24) can be approximated as

$$\bar{E}_0 \approx \frac{1}{R} \int_0^1 \Psi(Y) \bar{u}_{P0}(Y) dY. \quad (2.27)$$

From the definition of R , it can be deduced that \bar{E}_0 is proportional to ζ^2 . This indicates that the contribution of streaming potential to the velocity is of $O(\zeta^2)$ in (2.17). However, if fluid elasticity dominates the flow behaviour, resonances may occur and result in a very large increase in the amplitudes of the flow rate and streaming potential (figures 6 and 7). At this time, the effect of the streaming potential field on the velocity is significant and cannot be ignored (see figure 5 for high De). As a result, the approximation (2.27) and thereby the relationship $\bar{E}_0 \propto R^{-1}$ or $\bar{E}_0 \propto \zeta^2$ will no longer hold.

Figure 2 shows the variations of the maximum amplitude of streaming potential field, defined by $\bar{E}_{0,max} = \max|\bar{E}_0(\omega)|$, with the ionic Péclet number R^{-1} at different De . Here, the maximum amplitude occurs at the first-order resonance frequency (see figures 7a and 8b). At other frequencies, similar behaviour can also be observed. For comparison, both (2.24) and (2.27) are employed in figure 2. Using the physical properties $D = 1.9 \times 10^{-9} \text{ m}^2 \text{ s}^{-1}$, $\eta = 1.0 \times 10^{-3} \text{ kg m}^{-1} \text{ s}^{-1}$, $\varepsilon = 7 \times 10^{-10} \text{ C V}^{-1} \text{ m}^{-1}$ and $\zeta = 20 \text{ mV}$, we obtain $R \approx 7$. To extend the analysis, R is considered to range from 0.5 to 10 (equivalently, R^{-1} from 0.1 to 2). We observe that when the fluid viscosity dominates the flow behaviour (represented by low De), the variations of the streaming potential given by the two equations (2.24) and (2.27) are consistent, and a linear relationship, $\bar{E}_{0,max} \propto R^{-1}$, can be invoked as expected. However, the approximation (2.27) gradually fails with increasing De due to the occurrence of elastic resonance and significant deviations from

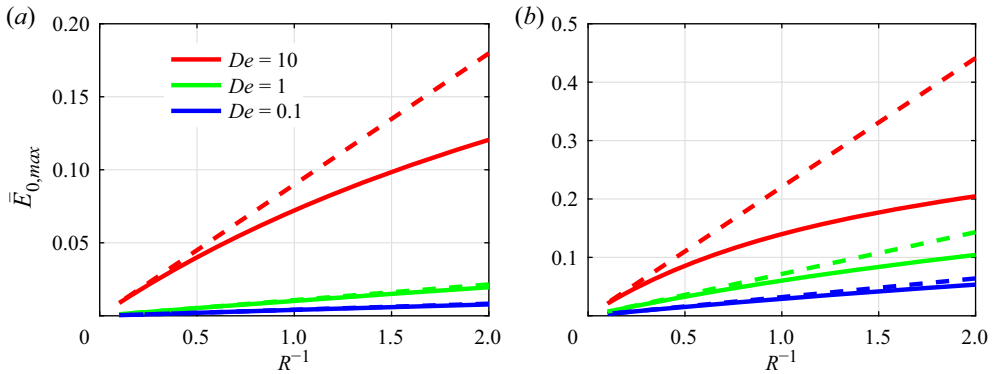


Figure 2. Scaling relations between the dimensionless streaming potential field and the ionic Péclet number R^{-1} at different Deborah number, where $\bar{E}_{0,max} = \max|\bar{E}_0(\omega)|$ with \bar{E}_0 provided by (2.24) (solid line) and the approximation (2.27) (dashed line). (a) $K = 15, X = 0$; (b) $K = 5, X = 0.1$.

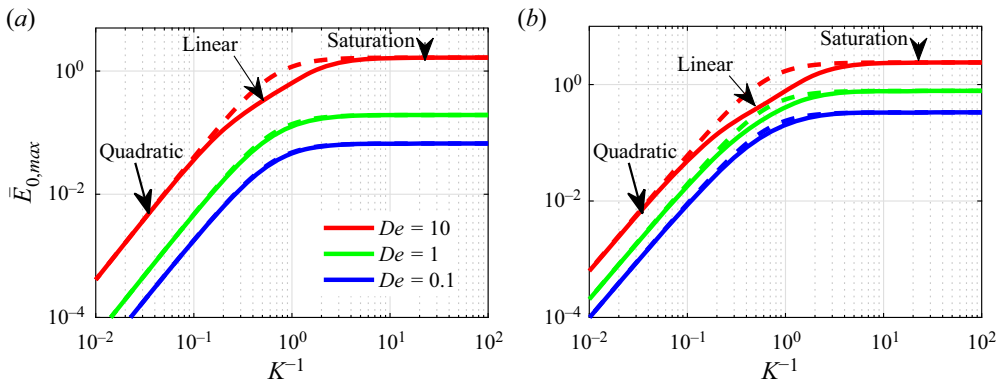


Figure 3. Scaling relations between the dimensionless streaming potential field and EDL thickness K^{-1} at different Deborah number, where $\bar{E}_{0,max} = \max|\bar{E}_0(\omega)|$ with \bar{E}_0 provided by (2.24) (solid line) and the approximation (2.27) (dashed line). (a) $R = 5, X = 0$; (b) $R = 1, X = 0.1$.

the linear relationship can be observed in the streaming potential field (the resonance behaviour is analysed in detail in § 3).

In figure 3, we show the scaling relations between the streaming potential field $\bar{E}_{0,max}$ and the dimensionless EDL thickness K^{-1} at different De . For viscous fluids (low De), there exist two distinct scaling regimes. For $K^{-1} < 1$, $\bar{E}_{0,max}$ increases with K^{-1} at $\bar{E}_{0,max} \sim K^{-2}$, which is termed the quadratic regime by Das *et al.* (2013). For $K^{-1} > 1$, i.e. large EDL thickness relative to the channel size, $\bar{E}_{0,max}$ is saturated and shows no further variation with K^{-1} . Hence, this regime is called the saturation regime (Das *et al.* 2013). When the elasticity of fluid is dominant (represented by high De , e.g. $De = 10$), a new regime, in addition to the above two, is observed. This regime occurs near $K^{-1} \approx 1$ (the onset of EDL overlap) and does not appear in the case of viscous fluids (see the dashed line in figure 3). In this third regime, $\bar{E}_{0,max}$ increases with K^{-1} at $\bar{E}_{0,max} \sim K^{-1}$. It is called the linear regime.

2.4. *Electrokinetic energy conversion*

Now, consider such a fluid system connected to an external load (with resistance R_L). Due to the establishment of streaming current and potential, the mechanical energy is converted into electric energy through the external load. This fluid system can be treated as a battery with an ideal current source plus an internal resistance R_{ch} , and an equivalent circuit has been presented (see, e.g. van der Heyden *et al.* 2007). The streaming current (I_s) is the current that passes through the circuit when the external resistance R_L is zero, i.e. I_s can be viewed as the short-circuit current in a circuit where the voltage $\Delta\phi$ is zero. The streaming potential ($\Delta\phi_s$) is equal to the voltage on R_L when the value of R_L is infinite, i.e. $\Delta\phi_s$ can be viewed as an open-circuit voltage in a circuit where the current I is zero. For a circuit, the instantaneous output power $W_{out} = I\Delta\phi$, where I is the current through R_L and $\Delta\phi$ is the voltage across R_L . Maximum power transfer occurs at $R_L = R_{ch}$ (Olthuis *et al.* 2005; van der Heyden *et al.* 2007). In that case, the current through the external load is half of the streaming current, i.e. $I = I_s/2$, and the voltage across R_L is half of the streaming potential, i.e. $\Delta\phi = \Delta\phi_s/2$. Note that in our system, the current and voltage vary with time. The time-averaged maximum output power over a cycle can be expressed as follows:

$$W_{out,max} = \frac{1}{4} \langle I_s \Delta\phi_s \rangle = \frac{\omega}{8\pi} \int_0^{2\pi/\omega} I_s(t) \Delta\phi_s(t) dt. \quad (2.28)$$

With the complex forms $I_s(t) = \text{Re}(I_{s0} e^{i\omega t}) = (I_{s0} e^{i\omega t} + I_{s0}^* e^{-i\omega t})/2$ and $E_s(t) = \text{Re}(E_0 e^{i\omega t}) = (E_0 e^{i\omega t} + E_0^* e^{-i\omega t})/2$ (* indicating complex conjugate), the expression $\Delta\phi_s(t) = -lE_s(t)$ with length l of the channel and $I_{s0} = -I_{c0} = -2h\sigma_b E_0$, we obtain

$$W_{out,max} = \frac{1}{4} h l \sigma_b |E_0|^2. \quad (2.29)$$

With the flow rate $Q = \text{Re}(Q_0 e^{i\omega t})$ through the channel under a pressure difference $\Delta p = l \partial p / \partial x = l \text{Re}(dp_0 / dx \exp(i\omega t))$, the time-averaged hydrodynamic power is given by

$$W_{in} = \langle Q(-\Delta p) \rangle = -\frac{l}{2} \frac{dp_0}{dx} \text{Re}(Q_0). \quad (2.30)$$

Note that the negative sign in the above expression is because the direction of fluid flow is consistent with that of pressure reduction. Furthermore, from (2.29), (2.30) and the non-dimensional forms (2.14) and (2.18), the efficiency of the maximum power transfer can be calculated:

$$\xi = \frac{W_{out,max}}{W_{in}} = \frac{RK^2 |\bar{E}_0|^2}{2 \text{Re}(\bar{Q}_0)}. \quad (2.31a)$$

It is worth noting that maximum EKEC efficiency has been defined and calculated in different ways in the literature. For example, Xuan & Li (2006) calculated the maximum conversion efficiency based on thermodynamics, whereas van der Heyden *et al.* (2006) calculated it based on the circuit. A few researchers (Chanda *et al.* 2014; Buren *et al.* 2018; Koranlou, Ashrafzadeh & Sadeghi 2019) defined the efficiency ξ in terms of a purely pressure-driven volume flow rate without the retardation induced by the back electro-osmotic transport.

In our recent study (Ding *et al.* 2019), we demonstrated the equivalence of thermodynamic and electric circuit analyses for calculating the maximum conversion efficiency in the linear response regime. Here, the calculation of maximum EKEC

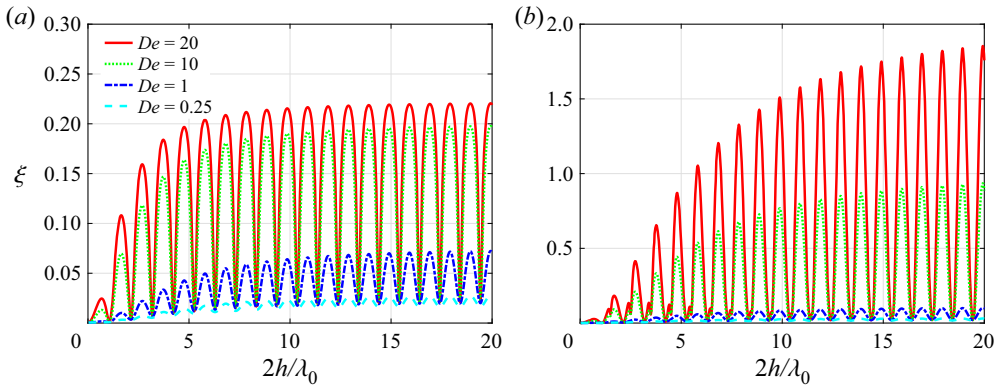


Figure 4. EKEC efficiencies calculated by different definitions for Maxwell fluids ($X=0$) at different De , where (a) the definition (2.31a) is used and (b) the definition (2.31b) with purely pressure-driven volume flow rate is used. Note that the meaning of the abscissa $2h/\lambda_0$ can be found in § 3.

efficiency based on the circuit is adopted. For comparison, we also express the maximum EKEC efficiency based on the purely pressure-driven flow rate as follows:

$$\xi' = \frac{1}{4} \frac{\langle I_s \Delta \phi_s \rangle}{\langle Q_p (-\Delta p) \rangle} = \frac{RK^2 |\bar{E}_0|^2}{2\text{Re}(\bar{Q}_{p0})}, \tag{2.31b}$$

where

$$\bar{Q}_{p0} = \frac{2De}{i\bar{\omega}} \left[1 - \frac{\tan(\alpha)}{\alpha} \right] \tag{2.32}$$

is the purely pressure-driven dimensionless flow rate (see also (2.18)).

For viscous fluids, because the effect of induced streaming potential on velocity is negligible compared with the effect of pressure gradient, $\bar{Q}_0 \approx \bar{Q}_{p0}$. Thus, the efficiencies calculated using (2.31a) and (2.31b) are approximately equal (Olthuis *et al.* 2005; Berli 2010; Ding *et al.* 2019). For viscoelastic fluids with resonance behaviour, the effect of streaming potential on the velocity cannot be ignored, and these two different definitions of EKEC efficiency result in significant differences. In particular, when (2.31b) is employed to calculate the EKEC efficiency, it predicts (incorrectly) maximum efficiency above 100 % (see figure 4), which violates the law of thermodynamics. This implies that the conversion efficiency defined by the purely pressure-driven flow rate does not apply to this condition.

3. Resonance phenomenon in electrokinetic transport

Bandopadhyay & Chakraborty (2012) predicted that EKEC efficiency may become greatly amplified due to the resonance phenomenon of viscoelastic fluids when subjected to a periodic external force. However, their model is valid only in a narrow range of parameters (e.g. low shear rates and frequencies), and the effects of resonance on the flow of liquid and streaming potential field in microfluidic channels are still unclear to a large extent. Using a viscoelastic fluid model that accounts for the effects of Newtonian solvent and multiple relaxation times, we address this issue at medium and high frequencies, which is especially important because the resonance phenomena usually occur in this range. It is worth noting that a low shear rate is still assumed in our situation so that the problem is in the linear regime, and thus it can be treated analytically.

The laminar oscillatory flows of single-mode Maxwell and Oldroyd-B fluids between two infinitely large parallel plates were analysed by Casanellas & Ortín (2011) from the perspective of viscoelastic shear waves. This perspective gives new physical insight, which is useful in understanding the mechanism of resonance phenomena. We employ this method to explore the resonance behaviour in periodic viscoelastic electrokinetic flows, and further extend it to the case of multimode oscillatory flows. First, we prove that the time-periodic pressure-driven electrokinetic flow is equivalent to the flow that results from synchronous oscillatory sidewalls with the same frequency, which is observed in the reference frame of the sidewalls. This proof is given in Appendix A. Note that this equivalence holds only in the linear regime (see Appendix A). Then, the flow can be regarded as the result of interference in the time and space of the shear waves generated by the oscillatory sidewalls. The dimensionless parameter α defined in (2.16) plays a key role in the analysis. Obviously, α is a complex number. It can be rewritten as

$$\alpha = \text{Re}(\alpha) + i \cdot \text{Im}(\alpha) = \frac{2\pi h}{\lambda_0} - i \frac{h}{x_0}, \tag{3.1}$$

where λ_0 and x_0 are the wavelength and damping length, respectively, of the transverse wave and are given by

$$\frac{\lambda_0}{2\pi} = \sqrt{\frac{2h^2 De}{\bar{\omega}}} \sqrt{\frac{\Omega_1^2 + \Omega_2^2}{\Omega_2 + \sqrt{\Omega_1^2 + \Omega_2^2}}}, \quad x_0 = \sqrt{\frac{2h^2 De}{\bar{\omega}}} \sqrt{\frac{\Omega_1^2 + \Omega_2^2}{-\Omega_2 + \sqrt{\Omega_1^2 + \Omega_2^2}}}, \tag{3.2a,b}$$

where

$$\Omega_1 = X + \sum_{k=1}^N \frac{\xi_k}{1 + (\omega\lambda_k)^2} \quad \text{and} \quad \Omega_2 = \sum_{k=1}^N \frac{\omega\lambda_k \xi_k}{1 + (\omega\lambda_k)^2}. \tag{3.3a,b}$$

The viscosity ratios X and ξ_k satisfy the relation $X + \sum_{k=1}^N \xi_k = 1$. Furthermore, we obtain that

$$\left| \frac{\text{Re}(\alpha)}{\text{Im}(\alpha)} \right| = \frac{2\pi x_0}{\lambda_0} = \frac{\Omega_2}{\Omega_1} + \sqrt{1 + \left(\frac{\Omega_2}{\Omega_1}\right)^2}. \tag{3.4}$$

The ratio $2\pi x_0/\lambda_0$ depends on the value of Ω_2/Ω_1 and is larger than unity, except for Newtonian fluids ($X = 1$), where $\xi_k = 0$, and thus $\Omega_2/\Omega_1 = 0$. In particular, for Maxwell fluids ($X = 0, N = 1$),

$$\left| \frac{\text{Re}(\alpha)}{\text{Im}(\alpha)} \right| = \frac{2\pi x_0}{\lambda_0} = \bar{\omega} + \sqrt{1 + \bar{\omega}^2} \gg 1 \text{ for large } \bar{\omega}. \tag{3.5}$$

The fact that this ratio is larger than unity is important and reveals that viscoelastic shear waves are always underdamped. In contrast, transverse oscillations of Newtonian fluids are overdamped, thereby making resonance impossible.

Now, we are concerned with the situation of resonance. From the expression of velocity (2.17), we deduce that resonance occurs at $\cos(\alpha) = 0$. From the Euler formula,

$$\cos(\alpha) = \frac{e^{i\text{Im}(\alpha)} + e^{-i\text{Im}(\alpha)}}{2} \cos(\text{Re}(\alpha)) + i \frac{e^{-i\text{Im}(\alpha)} - e^{i\text{Im}(\alpha)}}{2} \sin(\text{Re}(\alpha)), \tag{3.6}$$

so

$$\cos(\alpha) = 0 \quad \Leftrightarrow \quad \text{Im}(\alpha) = 0 \quad \text{and} \quad \text{Re}(\alpha) = n\pi - \frac{\pi}{2}, \quad n = 1, 2, \dots \tag{3.7}$$

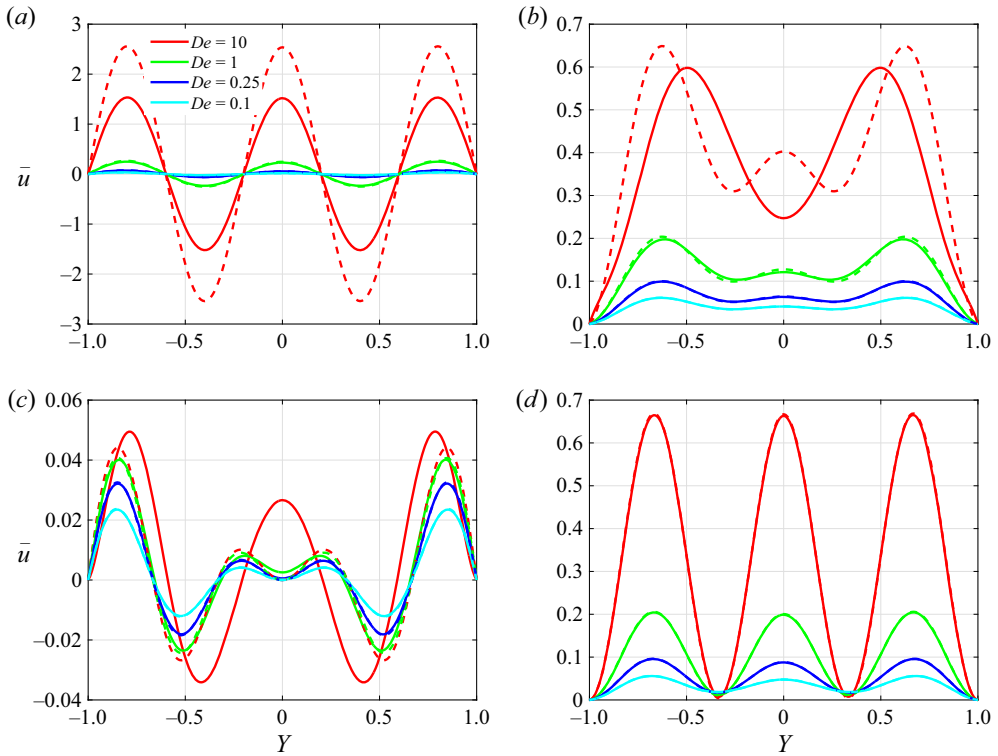


Figure 5. Normalised axial velocity profiles of Maxwell fluids ($X = 0$) across the channel at different De , with (solid line) and without (dashed line) the streaming potential effect. (a) $2h/\lambda_0 = 5/2$, $\omega t = 0$; (b) $2h/\lambda_0 = 5/2$, $\omega t = \pi/2$; (c) $2h/\lambda_0 = 3$, $\omega t = 0$; and (d) $2h/\lambda_0 = 3$, $\omega t = \pi/2$.

However, $\text{Im}(\alpha) = -h/x_0 = 0$ is an unrealistic requirement, so we resort to a weaker version:

$$\cos(\alpha) \approx 0 \quad \Leftrightarrow \quad |\text{Im}(\alpha)| \ll 1 \quad \text{and} \quad \text{Re}(\alpha) = n\pi - \frac{\pi}{2}, \quad n = 1, 2, \dots \quad (3.8)$$

Next, we analyse the meanings of the two conditions in (3.8) based on viscoelastic shear waves. Here, we introduce a viscoelastic Stokes parameter:

$$\Lambda_{ve} = \frac{h}{x_0} = |\text{Im}(\alpha)|, \quad (3.9)$$

as defined in Casanellas & Ortín (2011). This parameter Λ_{ve} represents the ratio of the transverse size of a system to the extension of the viscoelastic shear waves generated either by the oscillatory pressure gradient or by the moving sidewalls. ‘Narrow’ systems correspond to $\Lambda_{ve} < 1$, where the viscoelastic shear waves extend through the whole system, and ‘wide’ systems correspond to $\Lambda_{ve} > 1$, where the shear waves are attenuated at the centre of the channel. For ‘narrow’ systems, the viscoelastic shear waves generated at both plates are superposed, and they originate an interference pattern inside the fluid domain. This leads to resonance behaviour with a very large increase in the velocity amplitude at particular frequencies (see figure 5). In contrast, for ‘wide’ systems, the interaction of the shear waves is weak, viscous behaviour manifests and no resonance occurs. Thus, one of the conditions in (3.8) for resonance (i.e. $|\text{Im}(\alpha)| < 1$) implies a

‘narrow’ system from the perspective of viscoelastic shear waves. The other condition for resonance reads

$$\frac{2h}{\lambda_0} = n - \frac{1}{2}, \quad n = 1, 2, \dots, \quad (3.10)$$

which implies that the size of the channel $2h$ is a half-integer multiple of the wavelength λ_0 . Equation (3.10) indicates the constructive interference of the shear waves. The number n can be called the resonance order. In contrast, the condition

$$\frac{2h}{\lambda_0} = n, \quad n = 1, 2, \dots \quad (3.11)$$

implies the destructive interference of the shear waves. Further illustrations for the constructive and destructive interferences are given in [Appendix A](#).

From these conditions, it could be readily found that the resonance behaviour is closely related to the set-up dimensions, fluid parameters and applied driving frequency.

3.1. Single-mode Maxwell and Oldroyd-B fluids

To facilitate the analysis of the role of elasticity, we first investigate the resonance phenomenon in electrokinetic transport based on single-mode Maxwell and Oldroyd-B fluids. Such analyses are useful in the investigation of multimode viscoelastic fluids.

In these special cases, the wavelength and damping length of the transverse waves reduce to

$$\frac{\lambda_0}{2\pi} = \sqrt{\frac{2h^2 De}{\bar{\omega}}} \sqrt{\frac{1 + X^2 \bar{\omega}^2}{(1 - X)\bar{\omega} + \sqrt{(1 + \bar{\omega}^2)(1 + X^2 \bar{\omega}^2)}}} \quad (3.12)$$

and

$$x_0 = \sqrt{\frac{2h^2 De}{\bar{\omega}}} \sqrt{\frac{1 + X^2 \bar{\omega}^2}{(X - 1)\bar{\omega} + \sqrt{(1 + \bar{\omega}^2)(1 + X^2 \bar{\omega}^2)}}}, \quad (3.13)$$

which reproduce the results of Casanellas & Ortín (2011) for Oldroyd-B fluids (note the differences in the definitions and symbols of the dimensionless variables used). The viscoelastic Stokes parameter can be rewritten in terms of De , non-dimensional frequency $\bar{\omega}$ and solvent viscosity fraction X as follows:

$$\Lambda_{ve} = \frac{1}{\sqrt{De}} f(\bar{\omega}, X), \quad (3.14)$$

with

$$f(\bar{\omega}, X) = \sqrt{\frac{(X - 1)\bar{\omega}^2 + \bar{\omega}\sqrt{(1 + \bar{\omega}^2)(1 + X^2 \bar{\omega}^2)}}{2(1 + X^2 \bar{\omega}^2)}}. \quad (3.15)$$

Particularly, for Maxwell fluids ($X = 0$), we have

$$|f(\bar{\omega}, X = 0)| = \sqrt{\frac{\bar{\omega}\sqrt{(1 + \bar{\omega}^2)} - \bar{\omega}^2}{2}} = \sqrt{\frac{\bar{\omega}}{2(\sqrt{(1 + \bar{\omega}^2)} + \bar{\omega})}} \leq \frac{1}{2} \quad (3.16)$$

and

$$f(\bar{\omega}, X = 0) \approx \frac{1}{2} \text{ as } \bar{\omega} \gg 1. \quad (3.17)$$

As described by the Maxwell model, viscoelastic fluids have different flow regimes depending on the value of De (de Haro, del Río & Whitaker 1996; del Río *et al.* 1998).

A critical value, $De_c = 1/11.64$, which determines whether a dissipative behaviour prevails or a resonance appears at a given frequency, was obtained by de Haro *et al.* (1996) through numerical calculations for permeability in porous media. In this paper, we derive a different critical value of De from a physical point of view within parallel plate geometry. Based on the viscoelastic Stokes parameter (3.14) and the accurate bound (3.16), we deduce that

$$\Lambda_{ve} = \frac{h}{x_0} < 1 \quad \Leftrightarrow \quad De > \frac{1}{4} \quad (3.18)$$

for any $\bar{\omega}$ in the case of Maxwell fluids. Thus, the critical Deborah number can be obtained as $De_c = 1/4$. For small De ($De < De_c$), the damping length is small relative to the half-height of the channel and the conventional viscous effect dominates. However, beyond this critical value, the damping length is large relative to the half-height and the fluid system exhibits viscoelastic behaviour. These two flow regimes correspond to ‘wide’ and ‘narrow’ systems, respectively.

To gain some insight into the importance of the above analysis, we present some numerical calculations in the following illustrations, where the typical values of the parameters $K = 15$ and $R = 5$ have been adopted for microchannels (see (2.25) for the definition of R). The profiles of normalised axial velocity \bar{u} for Maxwell fluids at different De , with and without the streaming potential effect, are shown in figure 5. In figures 5(a) and 5(b), we show the velocity profiles that satisfy the third-order resonance condition (i.e. $2h/\lambda_0 = 5/2$) at two time phases, $\omega t = 0$ and $\omega t = \pi/2$, respectively. Figures 5(c) and 5(d) correspond to the destructive interference condition, $2h/\lambda_0 = 3$, at the same time phases ($\omega t = 0$ and $\omega t = \pi/2$, respectively). It can be found that for $De > De_c$, the elastic effect manifests and the oscillating profile is maintained from plate to plate, because of the large damping length. For larger De , the elastic effect is more significant. Furthermore, when the constructive interference condition (3.10) is satisfied simultaneously, resonance occurs and the amplitude of the velocity is greatly amplified. At resonance, the velocity is in phase with the harmonic pressure gradient, i.e. the velocity is maximum at $\omega t = 0$ and minimum at $\omega t = \pi/2$ (figure 5a,b). Conversely, outside the resonance (figure 5c,d), the velocity is nearly in quadrature with the pressure gradient and the behaviour is reversed, i.e. the velocity is maximum at $\omega t = \pi/2$ and minimum at $\omega t = 0$. In addition, at resonances, the presence of the streaming potential tends to decrease the magnitude of velocity, especially for large De . For example, the velocity is reduced by about 40% at $De = 10$ and $\omega t = 0$ (see figure 5a).

Figure 6 shows variations of the amplitude of the normalised flow rate at different De , where two variables are used as the horizontal axes. The appearance of elastic resonance behaviour depends on De . When $De > De_c$, resonance may occur at some special frequencies or values of $2h/\lambda_0$ (see (3.10)), whereas, for $De < De_c$, resonance does not occur and the flow rate amplitude drops rapidly to zero. As reported by Casanellas & Ortín (2011), the advantage of the choice of $2h/\lambda_0$ instead of the non-dimensional frequency $\bar{\omega}$, for the horizontal axis, is to make the location of the resonant peaks universal (independent of the fluid parameters and set-up dimensions). The increased frequency $\bar{\omega}$ corresponds to the reduced wavelength λ_0 and, thus, the increased ratio $2h/\lambda_0$. In the following illustrations, we adopt $2h/\lambda_0$ instead of the frequency as the horizontal axis, unless otherwise specified. It is observed that the resonance greatly enhances flow rate (several orders of magnitude higher than that of Newtonian fluids). The occurrence of resonance and its locations can be characterised under the conditions given in (3.18) and (3.10), respectively, regardless of whether the streaming potential effect is included (figure 6b). Besides, the streaming potential effect tends to suppress the resonance

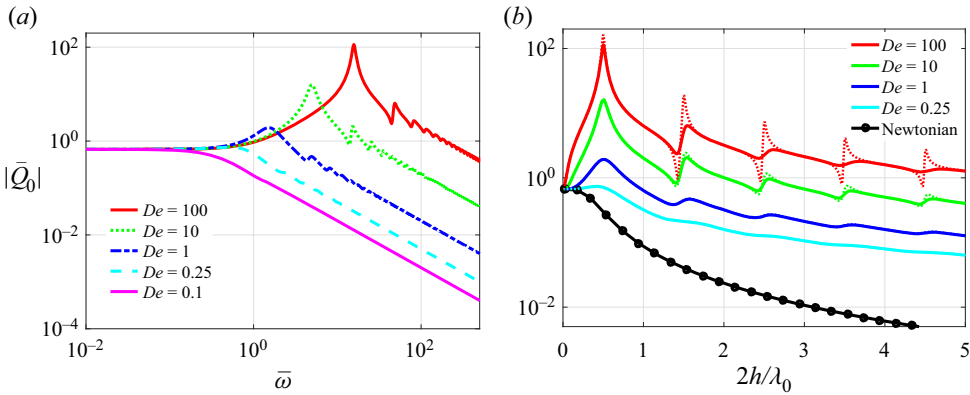


Figure 6. Variations of the non-dimensional flow rate of Maxwell fluids at different De , where two variables are used as the horizontal axis: (a) non-dimensional frequency $\bar{\omega}$; (b) $2h/\lambda_0$, with (solid line) and without (dashed line) the streaming potential effect. For comparison, the flow rate for Newtonian fluids ($De = 0$) is also plotted in (b).

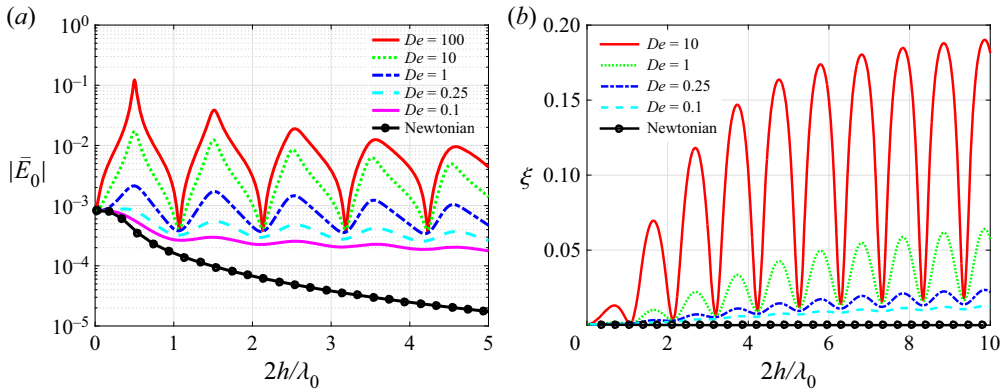


Figure 7. Resonance behaviours of (a) non-dimensional streaming potential and (b) EKEC efficiency ξ with $2h/\lambda_0$ for Maxwell fluids at different De .

behaviour and makes the flow rate vary smoothly with resonances, especially for large De .

Figure 7(a) shows the variations of the magnitude of the normalised streaming potential with $2h/\lambda_0$ at different De . The resonance behaviour of the streaming potential can be observed, and it is determined under the conditions in (3.10) and (3.18). At resonances, the amplitude of the streaming potential is greatly amplified, and it is further enhanced as De increases. This explains why the influence of the streaming potential is more pronounced at resonances, as shown in figure 6(b). The EKEC efficiency ξ for Maxwell fluids as a function of $2h/\lambda_0$ is depicted in figure 7(b). The viscoelastic behaviour of fluids improves the EKEC efficiency. The resonance further amplifies the efficiency by several orders of magnitude compared with that of Newtonian fluids. Here, the maximum efficiency is up to 19% in the range of the parameters. As shown in figures 6 and 7, as $2h/\lambda_0$ (or the frequency) increases, the peak values of the flow rate and streaming potential decrease. The maximum peak appears at the first-order resonance. However, this is not true for the EKEC efficiency; as the frequency increases, the peak values of the EKEC efficiency gradually increase and eventually tend to saturation (see figure 7b).

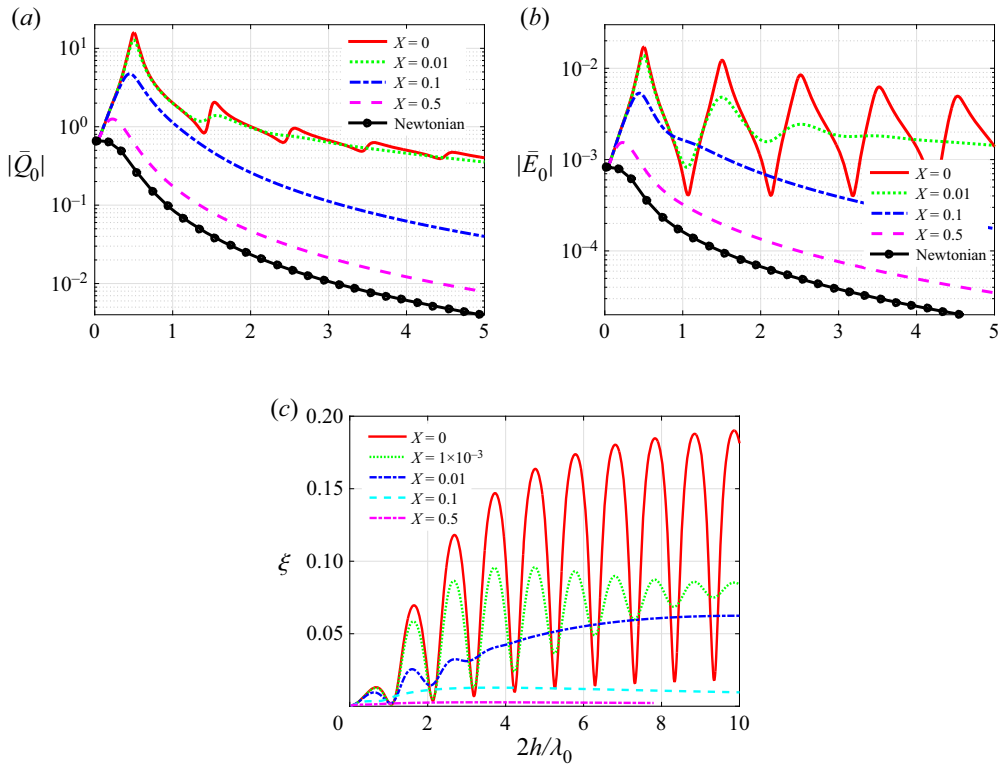


Figure 8. Variations of (a) non-dimensional flow rate, (b) non-dimensional streaming potential and (c) EKEC efficiency ξ with the ratio $2h/\lambda_0$ for Oldroyd-B fluid ($De = 10$). Different lines correspond to different values of the viscosity ratio X .

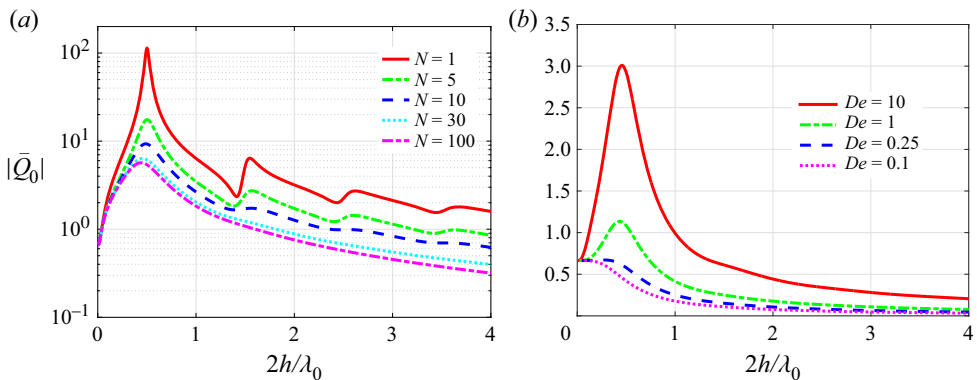


Figure 9. Variations of the non-dimensional flow rate for (a) different N ($De = 100$) and (b) different De ($N = 10$). Here the solvent viscosity effect is excluded ($X = 0$).

Figures 5–7 show the elastic resonance phenomena in the electrokinetic flow of Maxwell fluids ($X = 0$) driven by a periodic pressure gradient for different De . Next, we investigate the effect of solvent viscosity using the Oldroyd-B fluids model with positive viscosity ratio X for a fixed De (figure 8). Note that the critical De ($De_c = 1/4$) derived based on the Maxwell fluids model is still applicable to the case of Oldroyd-B fluids. As shown

in figure 8, the contribution of the Newtonian solvent tends to suppress the resonance behaviours of the flow rate and streaming potential in the electrokinetic flow. This is a result of viscous damping, and it has been observed in different contexts (Andrienko *et al.* 2000; Casanellas & Ortín 2011).

In particular, the high-order resonance phenomena are extremely sensitive to the effect of solvent viscosity. For a small ratio X of Newtonian solvent viscosity to the total viscosity of the solution (e.g. $X = 0.01$), the peaks corresponding to the high-order resonances are dramatically reduced and even disappear completely. Note that high-order resonances occur at high frequencies for fixed channel dimensions and fluid properties. This shows that the effect of solvent viscosity is more important in the high-frequency regime. Besides, the relatively large solvent viscosity effect (e.g. $X = 0.5$) results in a shift in the position of the first-order resonance to a lower frequency relative to the case of $X = 0$, as given in (3.10). Furthermore, EKEC efficiency is dramatically reduced due to the solvent viscosity effect. For example, the maximum efficiency drops rapidly from 19% to 6% when X increases from 0 to 0.01 at a fixed De of 10 (figure 8c). In electrokinetic flows of actual viscoelastic fluids (e.g. polymer solutions), the effect of the Newtonian solvent is inevitable (Yesilata *et al.* 2006). Hence, in practice, it is almost impossible to achieve the high efficiency predicted by Bandopadhyay & Chakraborty (2012) and Nguyen *et al.* (2017), although utilising the resonance behaviour of viscoelastic fluids can improve the energy conversion efficiency to some extent.

3.2. Multimode viscoelastic fluids

As explained in the Introduction section, using a multimode model allows a more realistic description of fluid memory by a spectrum of relaxation times. We consider the electrokinetic transport of multimode viscoelastic fluids with the constitutive equation (1.1). This model contains the constants λ_k and η_k ($k = 1, \dots, N$). We adopt the convention $\lambda_1 > \lambda_2 > \lambda_3 \dots$, and to reduce the total number of parameters, we employ the following expressions to generate the relaxation time and viscosity of each mode (Bird *et al.* 1987):

$$\lambda_k = \frac{\lambda}{k^\beta}, \quad \eta_k = \eta_0 \frac{\lambda_k}{\sum_k \lambda_k}, \quad (3.19a,b)$$

where η_0 is the zero-shear-rate viscosity, λ a time constant and β a dimensionless quantity. In our computations, we adopt $\beta = 2$, which approximates the value obtained from the Rouse molecular theory to dilute polymer solutions (Prost-Domasky & Khomami 1996). Note that in this model, $\eta_p = \sum \eta_k = \eta_0$, λ_k decreases as k increases and the largest relaxation time $\lambda_{max} = \lambda$.

Figure 9(a) shows the variations in the magnitude of the non-dimensional flow rate with $2h/\lambda_0$ for various N values. The peak values of resonances decrease with an increase in N . This can be attributed to the emergence of a relatively smaller relaxation time, and a role similar to that of the Newtonian solvent component is played by the smallest relaxation time for large N . As N increases, the peak values of high-order resonances dramatically reduce, and even disappear, whereas the first-order resonance behaviour can still be observed for $De > De_c$, although its peak value also decreases. However, unlike the solvent viscosity effect that causes a deviation in the resonance location, in the multimode case, the position of resonances is well characterised by condition (3.10), and no significant deviation occurs (see also figure 10). The dependence of the resonance behaviour of flow rate on De is displayed in figure 9(b). We observe that $De_c = 1/4$ derived from the single-mode Maxwell fluid model is still applicable to the multimode case.

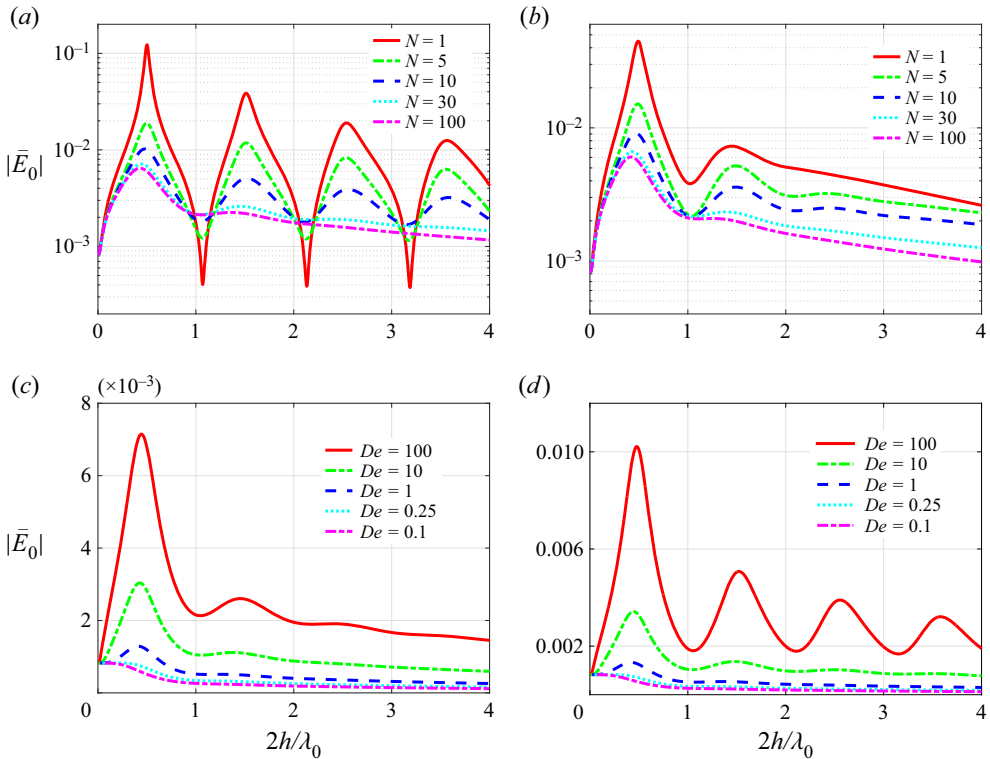


Figure 10. Variations of the non-dimensional streaming potential with $2h/\lambda_0$ for different parameters: (a) $De = 100, X = 0$; (b) $De = 100, X = 0.01$; (c) $N = 30, X = 0$; and (d) $N = 10, X = 0$.

When $De > De_c$, resonance occurs, whereas for $De < De_c$, the resonance disappears and the amplitude of the flow rate drops rapidly to zero with frequency.

The variations of the magnitude of the non-dimensional streaming potential and EKEC efficiency with $2h/\lambda_0$ for different parameters N, De and X are depicted in figures 10 and 11, respectively. Multiple relaxation times suppress the elastic resonance behaviours of the streaming potential and EKEC efficiency relative to those of single-mode Maxwell fluids. Similar to the flow rate, the occurrence of resonance in the streaming potential field is dominated by the critical Deborah number. When $De < De_c$, the resonance disappears and the amplitude of streaming potential field drops to zero with frequency (see figures 10c and 10d). This can be explained as follows: the largest relaxation time determines the elastic nature of the fluid; thus, the Deborah number defined based on the largest relaxation time can capture well the appearance of elastic resonance phenomena. However, in the multimode case, the occurrence of resonance for efficiency is complex. It is dominated by De and N . For small De or large N (e.g. $N > 10$ in figure 11), the resonance behaviour of efficiency disappears.

4. Validity of the linear analysis

In this paper, we investigate the electrokinetic phenomena of viscoelastic fluids driven by a periodic pressure gradient based on the multimode model, which includes the single-mode Maxwell and Oldroyd-B constitutive equations as particular cases. We assumed that the fluid is in laminar oscillatory flow so that the constitutive and motion equations of fluids

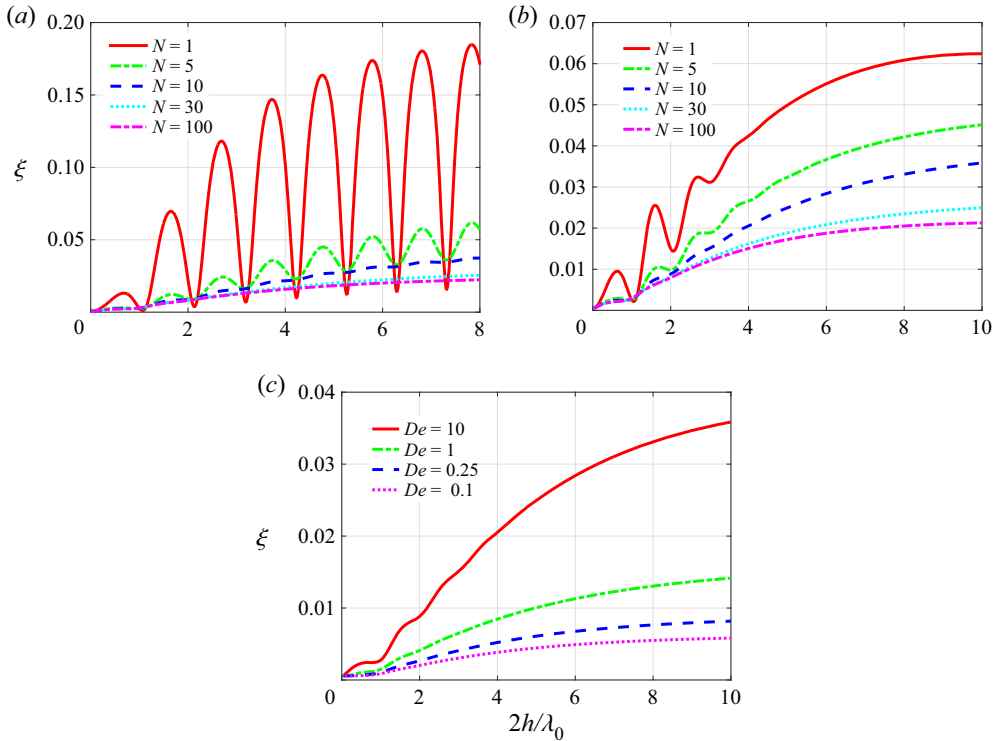


Figure 11. Variations of EKEC efficiency ξ with $2h/\lambda_0$ for multimode viscoelastic fluids at different values of N, X and De : (a) $De = 10, X = 0$; (b) $De = 10, X = 0.01$; and (c) $N = 10, X = 0.01$.

were reduced to the linear ones, and thus the fields of velocity and streaming potential can be solved analytically. Generally, the instability and transition of viscoelastic flows may occur in large-amplitude oscillatory shears, which depend on the geometry of the channel, Wi and Re . In microscale flows, Re is usually small and can be ignored. It is the Weissenberg number (Wi) that plays an important role in this basic geometry, and a critical Weissenberg number (Wi_c) related to the stability can be introduced. Typically, $Wi_c \sim O(1)$ (Torralba *et al.* 2007). For $Wi < Wi_c$, the fluid is expected to be in parallel shear flows with straight streamlines. Above this threshold nonlinearities and elastic instabilities start to become manifest. In this section, we investigate the validity of our linear analysis based on this threshold.

According to the definition, we have

$$Wi = \lambda_{max} \dot{\gamma}_{max} = \lambda_{max} \max \left\{ \left\| \frac{\partial u}{\partial y} \right\| \right\} = \frac{\lambda_{max} h}{\eta} \frac{dp_0}{dx} \max \left\{ \left\| \frac{d\bar{u}_0}{dY} \right\| \right\}, \quad (4.1)$$

where the local shear rate is computed by the velocity gradient and the dimensionless variables have been used. The dimensionless velocity gradient is readily available by differentiating (2.17). For simplicity, we first consider the case of single-mode fluids, i.e. $\lambda_{max} = \lambda$. Using the Cox–Merz rule, $\eta \simeq G_0 \lambda$ with a constant G_0 , an empirical relation that allows the relating of complex properties obtained under oscillatory shear experiments with steady shear flow measurements (Bird *et al.* 1987), we get

$$Wi = \frac{h}{G_0} \frac{dp_0}{dx} \left\| \frac{d\bar{u}_0}{dY} \right\|, \quad (4.2)$$

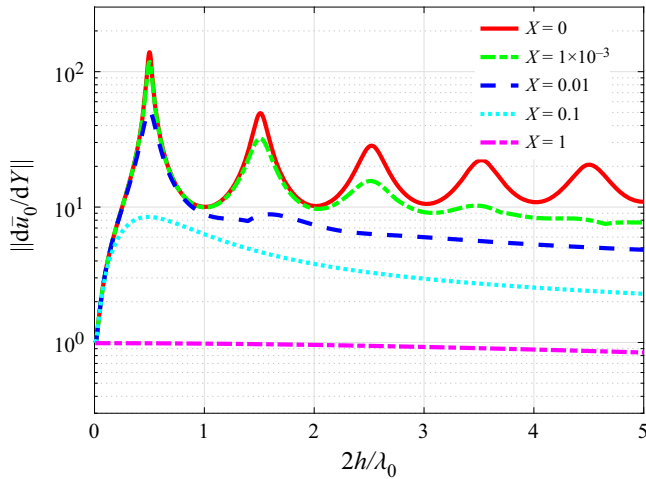


Figure 12. Variations of $\|d\bar{u}_0/dY\|$ with $2h/\lambda_0$ for single-mode viscoelastic fluids at different values of X ($De = 100$). Note that $X = 1$ corresponds to the Newtonian fluids case.

De	X	$\ d\bar{u}_0/dY\ $	Y_1	Δp^* (bar)
100	0	139.28	1	0.14
	0.001	118.58	0.95	0.17
	0.01	50.94	0.92	0.39
	0.1	8.45	0.97	2.37
	0.9	1.09	1	18.30
10	0	19.45	0.96	1.03
	0.001	19.00	0.96	1.05
	0.01	15.76	0.96	1.27
	0.1	6.10	0.98	3.28
	0.9	1.07	1	18.68

Table 1. Maximum values of the dimensionless velocity gradient at the first-order resonance for different De and X . Here Y_1 represents the position of the maximum value across the channel and Δp^* represents the maximum pressure difference applied to the system, where $Wi_c = 1$ has been used. Note that for $X = 0.9$, the fluid behaviour is close to that of Newtonian fluids.

with the norm $\|d\bar{u}_0/dY\| = \max\{|d\bar{u}_0(Y)/dY|\}$. Figure 12 illustrates the variations of $\|d\bar{u}_0/dY\|$ with $2h/\lambda_0$ for different values of X . Obviously, the peaks of the velocity gradient (or shear rate) are experienced at resonances, and the largest peak is at the first-order resonance. Furthermore, the largest values corresponding to different parameters are given in table 1. The constant G_0 depends on rheological properties of fluids, and its value varies from 0.45 to 30.2 Pa according to small-amplitude oscillatory shear experiments of wormlike micellar fluid samples (see Yesilata *et al.* 2006).

In order to keep the fluid response in the linear regime, the Weissenberg number is required to be less than the corresponding critical value, as stated above. This implies that the magnitude of the imposed pressure gradient must satisfy

$$\frac{dp_0}{dx} < \frac{G_0 Wi_c}{h} \left\| \frac{d\bar{u}_0}{dY} \right\|^{-1}. \tag{4.3}$$

Accordingly, the pressure difference through the channel is required to be less than Δp^* , where $\Delta p^* = lG_0 Wi_c \|d\bar{u}_0/dY\|^{-1}$ with l being the length of the channel. For illustrative computations, we consider the length (l) and height (h) of the channel to be 100 μm and 1 μm , respectively, and $G_0 = 20$ Pa. The results are shown in [table 1](#). It can be found that the value of $\|d\bar{u}_0/dY\|$ increases with De and decreases with X , which is consistent with the effects of parameters De and X on the viscoelastic behaviour. The maximum velocity gradient occurs near the walls (see [table 1](#)). The critical pressure difference, Δp^* , is small when the viscoelastic effect of fluids is significant (e.g. large De and very small X). However, when the fluid behaviour is close to that of Newtonian fluids, this critical value increases significantly.

Finally, we consider multimode viscoelastic fluids containing a spectrum of relaxation times ($N > 1$), where the resonance behaviour is weakened compared with the single-mode case ($N = 1$). The peaks of velocity gradient or shear rate at resonances are reduced. Therefore, the critical pressure difference that determines the fluid in laminar oscillating flows is increased compared with the single-mode case.

5. Summary and conclusions

In this study, we investigated the resonance phenomenon in the electrokinetic transport of viscoelastic fluids that include the realistic effects of Newtonian solvents and multiple relaxation times. Under some assumptions (e.g. low EDL potential and small Wi), the governing equations of fluid velocity and electric potential were reduced to a set of linear equations that can be solved analytically. In the analytical solutions, we introduced a complex dimensionless parameter α , which plays a key role in the analysis. With the equivalence between the time-periodic pressure-driven flow and the flow induced by synchronous oscillatory sidewalls in the linear regime, the meaning of α can be explained on the basis of viscoelastic shear waves generated by oscillatory sidewalls. Its real part represents the ratio of the height of the channel to the wavelength of the shear waves and the imaginary part represents the ratio of the half-height of the channel to the damping length of the shear waves. By means of the imaginary part of α , one can define a viscoelastic Stokes parameter that determines whether the waves generated at the opposite walls interfere. If interference occurs, its form (i.e. constructive or destructive interference) depends on the real part of α . When the conditions for constructive interference are satisfied, resonance appears. Furthermore, the following conclusions can be drawn.

First, based on the interaction of viscoelastic shear waves, we explained the mechanism of the resonance and obtained a critical Deborah number, $De_c = 1/4$, which dominates the occurrence of resonance and is universal for parallel plate geometries, regardless of whether the streaming potential effect is included. The streaming potential effect does not change the ‘locations’ of resonances but weakens their strength. Above this threshold (De_c), resonances appear at particular frequencies and result in a dramatic amplification of the amplitudes of the flow rate and streaming potential. Particularly, the resonances further amplify the EKEC efficiency by several orders of magnitude, compared with the case of Newtonian fluids. A maximum efficiency of approximately 19% can be achieved in the range of the parameters. Besides, the concept of resonance order was introduced to accurately describe the behaviour of resonances corresponding to different driving frequencies. The locations of resonant peaks with different orders are determined universally by $2h/\lambda_0$.

Second, the effect of solvent viscosity was examined using the Oldroyd-B fluid model. The Newtonian solvent contribution tends to suppress the resonance behaviours of the flow rate, streaming potential and EKEC efficiency in the electrokinetic flow. This is a result of viscous damping. For example, the maximum efficiency drops rapidly from 19 % to 6 % at an extremely small ratio of solvent to solution viscosity ($X = 0.01$). This implies that the solvent viscosity effect greatly hinders the realisation of high efficiency predicted by Bandopadhyay & Chakraborty (2012) and Nguyen *et al.* (2017). In addition, the high-order resonance phenomena are extremely sensitive to the effect of solvent viscosity. For small X , the peaks corresponding to the high-order resonance are dramatically reduced and even disappear.

Third, we investigated the streaming potential and EKEC of viscoelastic fluids using a multimode model that allows for a spectrum of relaxation times and viscosities. Multiple relaxation times showed an inhibitory effect on the elastic resonance behaviours for the streaming potential field and EKEC efficiency compared with those of the single-mode model. Their peak values at resonances decrease with an increase in the number of relaxation times in the spectrum, which is attributed to the emergence of a relatively smaller relaxation time. For the streaming potential field and flow rate, the occurrence of resonance behaviours is still dominated by De_c . The locations of resonances are also well characterised by $2h/\lambda_0$. In the multimode case, the occurrence of resonance behaviour for EKEC efficiency is complex. It is dominated by De and the mode number N . For small De or large N , the resonance behaviour of efficiency disappears.

Besides, we identified three distinct regimes for the scaling relations between the dimensionless streaming potential field $\bar{E}_{0,max}$ and EDL thickness K^{-1} at high De : when the EDL thickness is much less than the half-height of the channel (e.g. $K^{-1} < 0.1$), $\bar{E}_{0,max}$ exhibits a quadratic growth trend with respect to K^{-1} (quadratic regime); when the EDL thickness is comparable to the half-height of the channel (i.e. $K^{-1} \approx 1$), $\bar{E}_{0,max}$ increases linearly with K^{-1} (linear regime); for larger overlapped values of the EDL thickness (e.g. $K^{-1} > 10$), $\bar{E}_{0,max}$ saturates and does not vary with K^{-1} (saturation regime).

Finally, we examined the validity of the linear analysis, which requires small driving amplitudes. Based on a threshold Weissenberg number, the maximum pressure gradient (or pressure difference) applied to fluid systems can be estimated. If the driving amplitudes exceed this maximum value, nonlinear rheology (e.g. shear-thinning behaviour) becomes relevant and this demands further studies. Our future work will focus on the nonlinear features of elastic resonances in the electrokinetic flow of viscoelastic fluids.

Acknowledgements. The authors gratefully acknowledge the anonymous referees and the editor for their valuable comments and suggestions.

Funding. This work was supported by the National Natural Science Foundation of China (grant nos. 11902165 and 11772162), the Natural Science Foundation of Inner Mongolia Autonomous Region of China (2019BS01004) and the Inner Mongolia Grassland Talent (12000-12102408).

Declaration of interests. The authors report no conflict of interest.

Author ORCID.

 Yongjun Jian <https://orcid.org/0000-0003-0263-8422>.

Appendix A. Equivalence between time-periodic pressure-driven electrokinetic flow and flow induced by synchronous oscillatory sidewalls

The governing equations of fluid flow driven by a periodic pressure gradient are given by

$$\left. \begin{aligned} \rho \frac{\partial \mathbf{V}}{\partial t} + \rho(\mathbf{V} \cdot \nabla)\mathbf{V} &= -\nabla p + \nabla \cdot \mathbf{T} + \mathbf{F}_{EK}, \\ \mathbf{T} &= \mathbf{T}_s + \mathbf{T}_p, \\ \mathbf{T}_s &= \eta_s \dot{\boldsymbol{\gamma}}, \quad \mathbf{T}_p = \sum_{k=1}^N \mathbf{T}_k, \\ \mathbf{T}_k + \lambda_k \overset{\nabla}{\mathbf{T}}_k &= \eta_k \dot{\boldsymbol{\gamma}}, \end{aligned} \right\} \quad (\text{A1})$$

subject to the no-slip boundary conditions

$$\mathbf{V}|_{walls} = 0. \quad (\text{A2})$$

Here $\mathbf{F}_{EK} = \rho_e \mathbf{E}$ represents electric field force and $\dot{\boldsymbol{\gamma}} = \nabla \mathbf{V} + (\nabla \mathbf{V})^\dagger$ is the rate-of-strain tensor.

Under the assumption of unidirectional flow, (A1) and (A2) reduce to

$$\left. \begin{aligned} \rho \frac{\partial u}{\partial t} &= -\frac{\partial p}{\partial x} + \eta_s \frac{\partial^2 u}{\partial y^2} + \sum_{k=1}^N \frac{\partial \tau_k}{\partial y} + \rho_e E_s, \\ \left(1 + \lambda_k \frac{\partial}{\partial t}\right) \tau_k &= \eta_k \frac{\partial u}{\partial y}, \\ u|_{walls} &= 0, \end{aligned} \right\} \quad (\text{A3})$$

where $u(y, t)$ is the axial velocity and $\partial p/\partial x = A \cos(\omega t)$ is the harmonic pressure gradient independent of position. The nonlinear convection term in (A1) has vanished, and thus the problem is in the linear regime.

On the other hand, consider the electrokinetic flow induced by the synchronous oscillatory sidewalls with the same frequency. Under the same assumption of unidirectional flow, the governing equations can be written as

$$\left. \begin{aligned} \rho \frac{\partial \tilde{u}}{\partial t} &= \eta_s \frac{\partial^2 \tilde{u}}{\partial y^2} + \sum_{k=1}^N \frac{\partial \tau_k}{\partial y} + \rho_e E_s, \\ \left(1 + \lambda_k \frac{\partial}{\partial t}\right) \tau_k &= \eta_k \frac{\partial \tilde{u}}{\partial y}, \\ \tilde{u}|_{walls} &= B \sin(\omega t), \end{aligned} \right\} \quad (\text{A4})$$

where B is the amplitude.

After introducing the transformation $\tilde{u} = u + B \sin(\omega t)$ with $B = A/\rho\omega$, one can readily find that the equations in (A4) are the same as those in (A3). This implies that the time-periodic pressure-driven electrokinetic flow is equivalent to the flow that results from the synchronous oscillatory sidewalls with the same frequency, observed in the reference frame of the sidewalls. Here it is worth noting that the oscillating reference frame is not an inertial frame of reference. For an incompressible flow in which the density ρ is a constant, the inertial body force term $\rho\omega B \cos(\omega t)$, generated after the transformation $\tilde{u} = u + B \sin(\omega t)$ in (A4), can be regarded as a pressure gradient $\partial p/\partial x = \rho\omega B \cos(\omega t)$, and thus can be included in the Navier–Stokes equations, thereby recovering exactly the same formulation as in (A3) with fixed sidewalls. The above equivalence does not depend on the geometry of channel section. However, we point out that if beyond the linear regime (e.g. the convection term does not vanish), this equivalence will no longer hold.

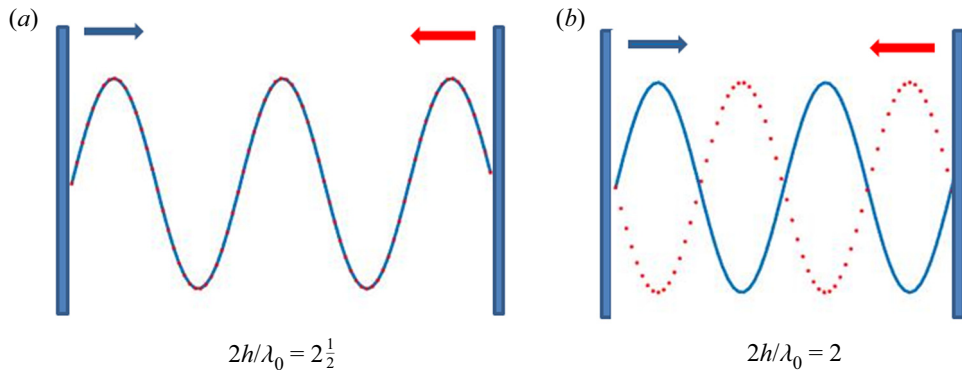


Figure 13. Schematic diagram for the interference phenomenon of viscoelastic shear waves generated at opposite walls. (a) The constructive interference of the shear waves where the size of the channel $2h$ is a half-integer multiple of the wavelength λ_0 . (b) The destructive interference of the shear waves where the size of the channel is an integer multiple of the wavelength. Here, the damping of shear waves is ignored and the arrows indicate the direction of wave propagation.

Based on this equivalence, the flow can be viewed as the result of the interference in time and space of the shear waves generated by the oscillatory sidewalls. In figure 13, we show a schematic diagram for the interference phenomenon of viscoelastic shear waves generated at opposite walls. Here, the damping of viscoelastic shear waves is ignored and we focus on the interference behaviour.

REFERENCES

- ANDRIENKO, Y.A., SIGINER, D.A. & YANOVSKY, Y.G. 2000 Resonance behavior of viscoelastic fluids in Poiseuille flow and application to flow enhancement. *Intl J. Non-Linear Mech.* **35** (1), 95–102.
- BANDOPADHYAY, A. & CHAKRABORTY, S. 2011 Steric-effect induced alterations in streaming potential and energy transfer efficiency of non-newtonian fluids in narrow confinements. *Langmuir* **27** (19), 12243–12252.
- BANDOPADHYAY, A. & CHAKRABORTY, S. 2012 Giant augmentations in electro-hydro-dynamic energy conversion efficiencies of nanofluidic devices using viscoelastic fluids. *Appl. Phys. Lett.* **101** (4), 043905.
- BARNES, H., TOWNSEND, P. & WALTERS, K. 1969 Flow of non-Newtonian liquids under a varying pressure gradient. *Nature* **224**, 585–587.
- BARNES, H., TOWNSEND, P. & WALTERS, K. 1971 Pulsatile flow of non-Newtonian liquids. *Rheol. Acta* **10**, 517–527.
- BERLI, C.L.A. 2010 Electrokinetic energy conversion in microchannels using polymer solutions. *J. Colloid Interface Sci.* **349** (1), 446–448.
- BIRD, R.B., ARMSTRONG, R.C. & HASSAGER, O. 1987 *Dynamics of Polymeric Liquids*, 2nd edn, vol. 1. John Wiley & Sons.
- BOCQUET, L. & CHARLAIX, E. 2010 Nanofluidics, from bulk to interfaces. *Chem. Soc. Rev.* **39**, 1073–1095.
- BOLÉVE, A., CRESPIY, A., REVIL, A., JANOD, F. & MATTIUZZO, J.L. 2007 Streaming potentials of granular media: influence of the Dukhin and Reynolds numbers. *J. Geophys. Res.* **112**, B08204.
- BUREN, M., JIAN, Y., ZHAO, Y. & CHANG, L. 2018 Electroviscous effect and electrokinetic energy conversion in time periodic pressure-driven flow through a parallel-plate nanochannel with surface charge-dependent slip. *J. Phys. D: Appl. Phys.* **51** (20), 205601.
- CASANELLAS, L. & ORTÍN, J. 2011 Laminar oscillatory flow of Maxwell and Oldroyd-B fluids: theoretical analysis. *J. Non-Newtonian Fluid Mech.* **166** (23–24), 1315–1326.
- CASANELLAS, L. & ORTÍN, J. 2012 Experiments on the laminar oscillatory flow of wormlike micellar solutions. *Rheol. Acta* **51**, 545–557.
- CASTREJÓN-PITA, J.R., DEL RÍO, J.A., CASTREJÓN-PITA, A.A. & HUELSZ, G. 2003 Experimental observation of dramatic differences in the dynamic response of Newtonian and Maxwellian fluids. *Phys. Rev. E* **68** (4), 046301.

- CHAKRABORTY, S. & DAS, S. 2008 Streaming-field-induced convective transport and its influence on the electroviscous effects in narrow fluidic confinement beyond the Debye-Hückel limit. *Phys. Rev. E* **77** (3), 037303.
- CHANDA, S., SINHA, S. & DAS, S. 2014 Streaming potential and electroviscous effects in soft nanochannels: towards designing more efficient nanofluidic electrochemomechanical energy converters. *Soft Matter* **10** (38), 7558–7568.
- CHANG, C.C. & YANG, R.J. 2011 Electrokinetic energy conversion efficiency in ion-selective nanopores. *Appl. Phys. Lett.* **99** (8), 083102.
- DAIGUJI, H., OKA, Y., ADACHI, T. & SHIRONO, K. 2006 Theoretical study on the efficiency of nanofluidic batteries. *Electrochem. Commun.* **8** (11), 1796–1800.
- DAIGUJI, H., YANG, P., SZERI, A. & MAJUMDAR, A. 2004 Electrochemomechanical energy conversion in nanofluidic channels. *Nano Lett.* **4** (12), 2315–2322.
- DAS, S., GUHA, A. & MITRA, S.K. 2013 Exploring new scaling regimes for streaming potential and electroviscous effects in a nanocapillary with overlapping electric double layers. *Anal. Chim. Acta* **804**, 159–166.
- DAVIDSON, C. & XUAN, X. 2008a Electrokinetic energy conversion in slip nanochannels. *J. Power Sources* **179** (1), 297–300.
- DAVIDSON, C. & XUAN, X. 2008b Effects of Stern layer conductance on electrokinetic energy conversion in nanofluidic channels. *Electrophoresis* **29** (5), 1125–1130.
- DAVIES, J., BHUMIRATANA, S. & BIRD, R. 1978 Elastic and inertial effects in pulsatile flow of polymeric liquids in circular tubes. *J. Non-Newtonian Fluid Mech.* **3**, 237–259.
- DE HARO, M.L., DEL RÍO, J.A.P. & WHITAKER, S. 1996 Flow of Maxwell fluids in porous media. *Trans. Porous Med.* **25** (2), 167–192.
- DEL RÍO, J.A., DE HARO, M.L. & WHITAKER, S. 1998 Enhancement in the dynamic response of a viscoelastic fluid flowing in a tube. *Phys. Rev. E* **58** (5), 6323–6327.
- DING, Z., JIAN, Y. & TAN, W. 2019 Electrokinetic energy conversion of two-layer fluids through nanofluidic channels. *J. Fluid Mech.* **863**, 1062–1090.
- GALINDO-ROSALES, F.J., CAMPO-DEAÑO, L., SOUSA, P.C., RIBEIRO, V.M., OLIVEIRA, M.S., ALVES, M.A. & PINHO, F.T. 2014 Viscoelastic instabilities in micro-scale flows. *Exp. Therm. Fluid Sci.* **59**, 128–139.
- GILLESPIE, D. 2012 High energy conversion efficiency in nanofluidic channels. *Nano Lett.* **12** (3), 1410–1416.
- GOSWAMI, P. & CHAKRABORTY, S. 2010 Energy transfer through streaming effects in time-periodic pressure-driven nanochannel flows with interfacial slip. *Langmuir* **26** (1), 581–590.
- GUAN, W., LI, S.X. & REED, M.A. 2014 Voltage gated ion and molecule transport in engineered nanochannels: theory, fabrication and applications. *Nanotechnology* **25** (12), 122001.
- HERRERA, E. 2010 Study on the pulsating flow of a worm-like micellar solution. *J. Non-Newtonian Fluid Mech.* **165** (3–4), 174–183.
- HUNTER, R.J. 2000 *Foundations of Colloid Science*, 2nd edn. Oxford University Press.
- JIAN, Y., LI, F., LIU, Y., CHANG, L., LIU, Q. & YANG, L. 2017 Electrokinetic energy conversion efficiency of viscoelastic fluids in a polyelectrolyte-grafted nanochannel. *Colloids Surf. B Biointerfaces* **156**, 405–413.
- KARNIADAKIS, G., BESKOK, A. & ALURU, N. 2005 *Microflows and Nanoflows: Fundamentals and Simulation*. Springer Science.
- KORANLOU, A., ASHRAFIZADEH, S.N. & SADEGHI, A. 2019 Enhanced electrokinetic energy harvesting from soft nanochannels by the inclusion of ionic size. *J. Phys. D: Appl. Phys.* **52**, 155502.
- LAC, E. & SHERWOOD, J.D. 2009 Streaming potential generated by a drop moving along the centreline of a capillary. *J. Fluid Mech.* **640**, 55–77.
- LI, D. 2004 *Electrokinetics in Microfluidics*, vol. II. Academic Press.
- LYKLEMA, J. 1995 *Fundamentals of Interface and Colloid Science*, vol. II. Academic Press.
- MANERO, O. & WALTERS, K. 1980 On elastic effects in unsteady pipe flows. *Rheol. Acta* **19**, 277–284.
- MASLIYAH, J.H. & BHATTACHARJEE, S. 2006 *Electrokinetic and Colloid Transport Phenomena*. John Wiley & Sons.
- MEI, L., YEH, L.-H. & QIAN, S. 2017 Buffer anions can enormously enhance the electrokinetic energy conversion in nanofluidics with highly overlapped double layers. *Nano Energy* **32**, 374–381.
- MOROZOV, A.N. & VAN SAARLOOS, W. 2007 An introductory essay on subcritical instabilities and the transition to turbulence in visco-elastic parallel shear flows. *Phys. Rep.* **447**, 112–143.
- MOYERS-GONZALEZ, M.A., OWENS, R.G. & FANG, J. 2008 A non-homogeneous constitutive model for human blood. Part I. Model derivation and steady flow. *J. Fluid Mech.* **617**, 327–354.

- MOYERS-GONZALEZ, M.A., OWENS, R.G. & FANG, J. 2009 On the high frequency oscillatory tube flow of healthy human blood. *J. Non-Newtonian Fluid Mech.* **163** (1–3), 45–61.
- MUNSHI, F. & CHAKRABORTY, S. 2009 Hydroelectrical energy conversion in narrow confinements in the presence of transverse magnetic fields with electrokinetic effects. *Phys. Fluids* **21** (12), 122003.
- NGUYEN, T., XIE, Y., DE VREEDE, L.J., VAN DEN BERG, A. & EIJKEL, J.C.T. 2013 Highly enhanced energy conversion from the streaming current by polymer addition. *Lab on a Chip* **13** (16), 3210–3216.
- NGUYEN, T., VAN DEN MEER, D., VAN DEN BERG, A. & EIJKEL, J.C.T. 2017 Investigation of the effects of time periodic pressure and potential gradients on viscoelastic fluid flow in circular narrow confinements. *Microfluid Nanofluid* **21** (3), 37.
- OLTHUIS, W., SCHIPPERS, B., EIJKEL, J. & VAN DEN BERG, A. 2005 Energy from streaming current and potential. *Sensors Actuators, B Chem.* **111**, 385–389.
- OSTERLE, J.F. 1964 Electrokinetic energy conversion. *J. Appl. Mech.* **31** (2), 161–164.
- PATWARY, J., CHEN, G. & DAS, S. 2016 Efficient electrochemomechanical energy conversion in nanochannels grafted with polyelectrolyte layers with pH-dependent charge density. *Microfluid Nanofluid* **20** (2), 37.
- PENNATHUR, S., EIJKEL, J.C.T. & VAN DEN BERG, A. 2007 Energy conversion in microsystems: is there a role for micro/nanofluidics? *Lab on a Chip* **7** (10), 1234–1237.
- PHAN-THIEN, N. 1978 Pulsating flow of polymeric fluids. *J. Non-Newtonian Fluid Mech.* **4**, 167–176.
- PHAN-THIEN, N. 1980 Flow enhancement mechanisms of a pulsating flow of non-Newtonian liquids. *Rheol. Acta* **19**, 285–290.
- PHAN-THIEN, N. 1981 On a pulsating flow of polymeric fluids: strain-dependent memory kernels. *J. Rheol.* **25**, 293–314.
- PHAN-THIEN, N. & DUDEK, J. 1982a Pulsating flow revisited. *J. Non-Newtonian Fluid Mech.* **11**, 147–161.
- PHAN-THIEN, N. & DUDEK, J. 1982b Pulsating flow of a plastic fluid. *Nature* **296**, 843–844.
- PROST-DOMASKY, S.A. & KHOMAMI, B. 1996 A note on start-up and large amplitude oscillatory shear flow of multimode viscoelastic fluids. *Rheol. Acta* **35** (3), 211–224.
- REN, Y. & STEIN, D. 2008 Slip-enhanced electrokinetic energy conversion in nanofluidic channels. *Nanotechnology* **19** (19), 195707.
- RUSSEL, W.B. 1978 The rheology of suspensions of charged rigid spheres. *J. Fluid Mech.* **85** (2), 209–232.
- SADEK, S.H. & PINHO, F.T. 2019 Electro-osmotic oscillatory flow of viscoelastic fluids in a microchannel. *J. Non-Newtonian Fluid Mech.* **266**, 46–58.
- SCHNITZER, O., FRANKEL, I. & YARIV, E. 2012 Streaming-potential phenomena in the thin-Debye-layer limit. Part 2. Moderate-Péclet-number theory. *J. Fluid Mech.* **704**, 109–136.
- SCHNITZER, O. & YARIV, E. 2016 Streaming-potential phenomena in the thin-Debye-layer limit. Part 3. Shear-induced electroviscous repulsion. *J. Fluid Mech.* **786**, 84–109.
- SCHOCH, R.B., HAN, J. & RENAUD, P. 2008 Transport phenomena in nanofluidics. *Rev. Mod. Phys.* **80** (3), 839–883.
- SHERWOOD, J.D. 1980 The primary electroviscous effect in a suspension of spheres. *J. Fluid Mech.* **101** (3), 609–629.
- SHERWOOD, J.D. 2007 Streaming potential generated by two-phase flow in a capillary. *Phys. Fluids* **19**, 053101.
- SHERWOOD, J.D. 2008 Streaming potential generated by a long viscous drop in a capillary. *Langmuir* **24** (18), 10011–10018.
- SHERWOOD, J.D. 2009 Streaming potential generated by a small charged drop in Poiseuille flow. *Phys. Fluids* **21**, 013101.
- SIGINER, A. 1991 On the pulsating pressure gradient driven flow of viscoelastic liquid. *J. Rheol.* **35**, 271–311.
- SIRIA, A., PONCHARAL, P., BIANCE, A.L., FULCRAND, R., BLASE, X., PURCELL, S.T. & BOCQUET, L. 2013 Giant osmotic energy conversion measured in a single transmembrane boron nitride nanotube. *Nature* **494** (7438), 455–458.
- SPARREBOOM, W., VAN DEN BERG, A. & EIJKEL, J.C.T. 2010 Transport in nanofluidic systems: a review of theory and applications. *New J. Phys.* **12** (3), 338–346.
- TORRALBA, M., CASTREJÓN-PITA, A.A., HERNÁNDEZ, G., HUELSZ, G., DEL RÍO, J.A. & ORTÍN, J. 2007 Instabilities in the oscillatory flow of a complex fluid. *Phys. Rev. E* **75** (5), 056307.
- VAN DER HEYDEN, F.H., BONTHUIS, D.J., STEIN, D., MEYER, C. & DEKKER, C. 2006 Electrokinetic energy conversion efficiency in nanofluidic channels. *Nano Lett.* **6** (10), 2232–2237.
- VAN DER HEYDEN, F.H., BONTHUIS, D.J., STEIN, D., MEYER, C. & DEKKER, C. 2007 Power generation by pressure-driven transport of ions in nanofluidic channels. *Nano Lett.* **7** (4), 1022–1025.
- WANG, M. & KANG, Q. 2010 Electrochemomechanical energy conversion efficiency in silica nanochannels. *Microfluid Nanofluid* **9** (2–3), 181–190.

Electrokinetic oscillatory flow and energy conversion

- XUAN, X. & LI, D. 2006 Thermodynamic analysis of electrokinetic energy conversion. *J. Power Sources* **156** (2), 677–684.
- YANG, J., LU, F., KOSTIUK, L.W. & KWOK, D.Y. 2003 Electrokinetic microchannel battery by means of electrokinetic and microfluidic phenomena. *J. Micromech. Microengng* **13**, 963–970.
- YARIV, E., SCHNITZER, O. & FRANKEL, I. 2011 Streaming-potential phenomena in the thin-Debye-layer limit. Part I. General theory. *J. Fluid Mech.* **685**, 306–334.
- YESILATA, B., CLASEN, C. & MCKINLEY, G.H. 2006 Nonlinear shear and extensional flow dynamics of wormlike surfactant solutions. *J. Non-Newtonian Fluid Mech.* **133** (2–3), 73–90.